Native and irradiation-induced defects in graphene: What can we learn from atomistic simulations?

J. Kotakoski* and A. V. Krasheninnikov

Division of Materials Physics, University of Helsinki

P.O. Box 42 (Pietari Kalmin katu 2), 00014 Helsinki, Finland

*email: jani.kotakoski@iki.fi

May 28, 2010

Abstract

Defects in graphene, a recently discovered one-atom-thick material with exceptional characteristics, may considerably alter its properties and have negative effects on the operation of graphene-based electronic devices. Defects, when deliberately created by ion and especially electron irradiation with a high spatial resolution, may also have a beneficial effect on the target. Thus the complete understanding of the energetics and dynamics of defects in graphene is required for engineering the properties of graphene-based materials and devices. In this Chapter we give an overview of the recent progress in the understanding of the role of defects in these materials. We briefly dwell on the experimental data on native and irradiation-induced defects in graphene, and give detailed account of recent simulation results for point and line defects in graphene. We also discussed at length the mechanisms of defect formation under ion and electron irradiation as revealed by atomistic computer simulations.

Contents

1 Introduction

Graphene – the ultimately thin honeycomb-like membrane consisting only of sp^2-bonded carbon atoms – has been one of the most attractive research subjects since mono-layer graphene flakes became available for experiments.[1] Indeed, the yearly number of publications which mention graphene (see Fig. 1) demonstrates an exponential growth. A considerable part of these publications are theoretical studies, and the general consensus is that at the moment experimental understanding lags behind theory. This is because graphene has been simulated by the computational materials science community well before it was experimentally discovered. In fact, the electronic properties of this material were addressed for the first time more than 60 years ago.[2] The reason for the early interest arose from the fact that the most stable carbon allotrope, graphite, is formed by stacking a large number of graphene layers on top of each other to obtain the bulk structure kept together by weak van der Waals forces between the individual layers. Thus, to understand the physics and chemistry

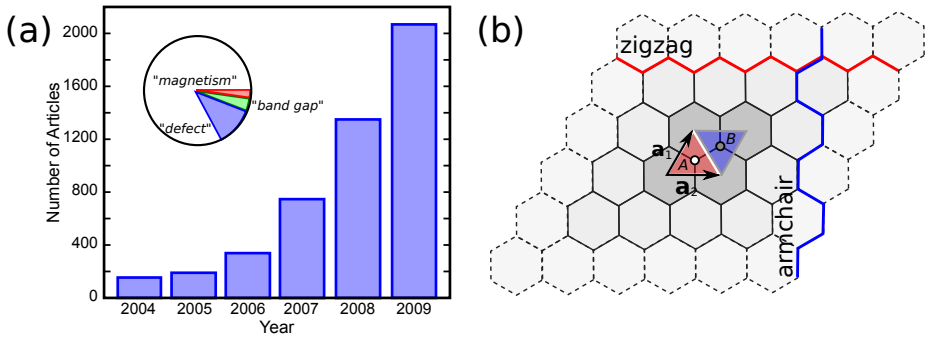

Figure 1: Number of publications per year (a) which are found with the ISI Web of Knowledge (published by Thomson Reuters) search at `http://isiknowledge.com/` with search term "*graphene*" since the first report on experiments on mono-layer graphene in 2004. The piechart shows how many of those publications were associated with search terms "*magnetism*", "*band gap*" or "*defect*", the last of which was combined with other related keywords. Note that some publications are likely to be found in more than one category. Graphene honeycomb lattice (b) with the two triangular sublattices A and B marked along with the lattice vectors $\mathbf{a}_1$ and $\mathbf{a}_2$, as well as zigzag and armchair lattice directions in the structure.

of graphite, one must first study graphene as the prototype material.

Humankind has used graphite in paints for centuries because the layers can easily be detached from another and used to mark surfaces with a dark color. More recently, graphite has been utilized in pencils and as a lubricant for the same reason. In contrast to the weak inter-layer interaction, the intra-layer sp^2 carbon bonds are among the strongest bonds known in nature – even stronger than the sp^3-bonds of diamond. Carbon is famous for the most complicated chemistry possible for any element, which has – as an extreme example – allowed the evolution of life on Earth through the DNA molecule. It has four valence electrons which occupy the $2s$ (two electrons), and $2p$ orbitals. In compounds, carbon exists in different sp-hybridizations, such as sp^1, sp^2 and sp^3, where the superscript denotes the number of $2p$ orbitals involved in bonding. Of these, sp^1 leads to a 1D chain, sp^2 to 2D graphene and sp^3 to 3D diamond. The left-over orbitals do not take part in the bonding. Surprisingly, graphite was also found to exhibit peculiar electronic properties (*e.g.* conductivity similar to that of a poor metal, negative temperature coefficient). When the rise of quantum mechanics

made it possible to understand the electronic structure of materials, scientists set out to find the underlaying reason for these properties. The early work of Wallace[2] applied a tight binding (TB) model to the π electrons of the sp^2-bonded graphene mono-layer, and showed that this material is a *zero-band gap semiconductor* (or in other words, a *semi-metal*) with unusual linearly dispersing electronic excitations reminiscent of relativistic Dirac electrons. However, the role of electron-electron interactions in graphene is still a subject of intensive research. The latest developments in the theory of the electronic structure of graphene can be found in a recent review by Castro Neto *et al.*.[3]

However, not only the academic interest has been the driving force for intensive research of the electronic properties of graphene. Our time is sometimes referred to as the Information Age, and we indeed rely heavily on the ever-increasing computational power. This has been made possible due to the success of materials science in miniaturizing silicon-based electronic components (mainly transistors) and increasing the speed of their operation. As the atomic scale is being approached, it has become evident that new materials are needed to retain the computational speed increase and circumvent the fundamental size-related problems. Graphene and other nano-scale carbon materials, with their extraordinary properties,[3;4] have been proposed for this purpose.

An important aspect regarding electronic properties is the effect of disorder. This is particularly relevant to graphene grown with the chemical vapor deposition (CVD) method. The CVD graphene is known to contain a large number of dislocations and disordered areas, some of which may originate from the growth processes, and some from imaging the structure[5] in a transmission electron microscope. In addition to native, pre-existing defects, defects can also be introduced via irradiation (*e.g.* in outer space, nuclear reactors) or created in a chemically harsh environment (*e.g.* by oxidation). Impacts of energetic particles such as electrons or ions typically give rise to formation of atomic defects in solids, sometimes making the material unusable for a particular application. Historically, the necessity of understanding irradiation effects in carbon mate-

rials emerged during the 1950's with the appearance of nuclear power plants in which the irradiation-induced degradation of graphitic components was an important issue (see Ref.[6] for an example). ISI Web of Knowledge lists 4 research articles with search terms "*graphite*" and "*irradiation*" during the 1950's, and 56 in the 1960's. After this the number has steadily increased until the early 1990's, after which it exploded to reach 1054 during the first decade of this century. The exponential growth in the number of publications occurs at the same time as the appearance of carbon nanotube publications (carbon nanotubes were brought to common knowledge in 1991[7]). During all these decades, also electron irradiation has been used to study the radiation damage effects in graphitic materials.

Despite the detrimental effects irradiation has on the target, beams of energetic particles can also be used for tailoring material properties. The most obvious example is ion implantation technology customarily employed in semiconductor industry.[8] Computer simulations have shown[9;10] that it is possible to use ion irradiation to replace carbon atoms by boron and nitrogen via ion irradiation to either dope or functionalize a carbon nanotube. Experiments have confirmed these results.[11;12] In graphene, due to the lack of curvature, this process can be expected to be even easier. Experiments have also demonstrated that the morphology of graphene can be changed in a controllable manner using electron irradiation.[13–15] While structural defects are known to alter the electronic properties of carbon nanomaterials,[16;17] this opens up the possibility for creating nanoscale devices for electronics from graphene.

In general, nanomaterials have a drastically different response to radiation with respect to the bulk counterparts because of their dimensions; an energetic particle typically passes through a nanostructure without depositing all of its energy into the system. Moreover, the displaced target atoms customarily become ejected out from the nanostructure instead of contributing to a collision cascade. Thus, both the primary and secondary collisions in nanostructures differ from those in bulk. Especially in the case of a monatomic layer, such

as graphene, the conventionally used models for estimating irradiation damage in solids fail, as demonstrated in Ref.[18] The difference in deposited energies to nanostructures and bulk under irradiation means that using irradiation in a useful manner to modify nanostructures is possible with less damage as compared to bulk structures. Despite a few recent studies,[19–22] no experiments have yet revealed ion irradiation effects in graphene at the microscopic level. Therefore, computational work is needed as a guidance for the later experiments. Also the microscopic processes occurring under electron irradiation of graphene have remained unknown, as will be explained in this Chapter.

In this Chapter, we give an overview of recent theoretical progress in our understanding of native and irradiation-induced defects in graphene with a particular stress on the theoretical results. We first discuss the observed electron- and ion-bombardment–mediated effects in graphene, and outline the experimental techniques used to characterize these effects. Then, computational methods employed to simulate irradiation of graphene are briefly introduced. We then describe the variety of defects which exist in this material either naturally or due to irradiation. Finally, we explain how irradiation can be used to modify the properties of graphene, and why atomistic simulations play a crucial role in understanding the active microscopic processes.

2 Experimental evidence for defects in graphene

2.1 Transmission-electron microscopy (TEM) and defects created by the electron beam

Discussing recent scientific progress in understanding the physics of sp^2-bonded carbon, and especially graphene, without considering high resolution transmission electron microscopy (HR-TEM) is – if not meaningless – at least disingenuous. HR-TEM is currently the ultimate device for atomic scale imaging. It offers a two-dimensional projection of the target material – with an atomic resolution if the device is aberration corrected. Clearly, for such a device, the

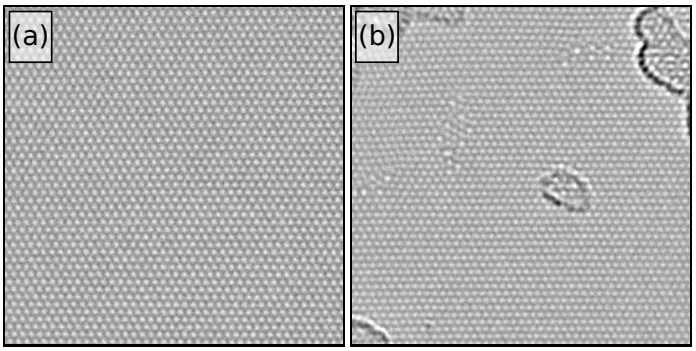

Figure 2: HR-TEM images of graphene. When the acceleration voltage is below the threshold for defect production, no damage is created during imaging (a). Brief exposure of graphene to high energy electron irradiation creates a set of complex defect structures built from a random set of polygons (b) with a locally slightly lowered density due to ejected atoms. Images courtesy of Jannik Meyer, University of Ulm, Germany.

optimal target material would be a two-dimensional atomically thin membrane, *e.g.* graphene. For such a target it is possible to see each individual atom if the local atomic configuration under the electron beam remains stationary during the exposure, as shown in Fig. 2. This property can also be used in utilizing graphene as the thinnest possible TEM grid material for HR-TEM experiments; when carbon atoms in the lattice are stationary, their positions can be extracted from the TEM images completely.[14] The stability of the atomic structure under the beam (its radiation hardness) depends on possible pre-existing defects, environment (for example foreign molecules present in the TEM vacuum chamber), and the acceleration voltage of the TEM. When displacements of target atoms occur due to electron impacts, it is impossible to follow the motion of the atoms *in situ* because of the difference between the time scale of displacement events (10^{-21} s) and exposure times (1 s).[23] The first HR-TEM images of graphene have revealed both the perfect honeycomb structure as well as various defects.[13–15;24]

In the case of graphene, electron irradiation clearly cannot be used to introduce such drastic structural changes as has been demonstrated for other carbon nanomaterials (*e.g.* using carbon nanotubes and onions as pressure vessels by

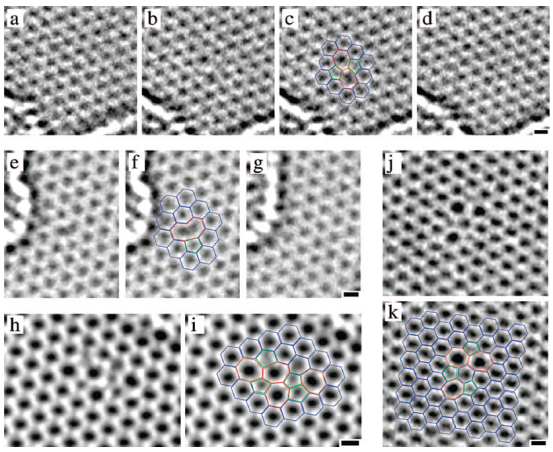

Figure 3: Metastable defects found in HRTEM image sequences. (a-d) Stone-Wales (SW) defect: (a) unperturbed lattice before appearance of the defect, (b) SW defect (c) same image with atomic configuration superimposed, (d) relaxation to unperturbed lattice (after ca. 4 s). (e-g) Reconstructed vacancy: (e) original image and (f) with atomic configuration; a pentagon is indicated in green. (g) Unperturbed lattice, 4 s later. (h and i) Defect image and configuration consisting of four pentagons (green) and heptagons (red). Note the two adjacent pentagons. (j and k) Defect image and configuration consisting of three pentagons (green) and three heptagons (red). This defect returned to the unperturbed lattice after 8 s. In spite of the odd number of 5-7 pairs, this is not a dislocation core (it is compensated by the rotated hexagon near the center of the structure). All scale bars are 2 Å. From Ref.[14]

decreasing their diameter under a TEM beam.[25;26]) However, there are ways to also alter the morphology of graphene with a TEM. For example, reorganization of edges of large holes has been shown (Fig. 4).[15] With electron irradiation, under conditions where graphene cannot compensate the loss of atoms via bond rotations, creation of holes and deriving monatomic carbon chains between two such holes has been demonstrated.[27;28] Overall, energetic electrons will cause significant changes to the atomic network after a sufficient dose by introducing a randomized polygon structure in the place of the honeycomb lattice. Typical result of continuous electron irradiation with a high enough acceleration voltage (∼100 kV) is shown in Fig. 2(b). Curiously, most atoms remain three-coordinated with sp^2-hybridization. Hence, the structure also remains truly two-dimensional. In the defected regions some atoms are missing and the lattice has accommodated the locally lowered density by reorganizing the atoms. The kinetic energy which allows for the reorganization is provided by the electron beam via knock-on collisions with target atoms.

2.2 Defects produced by ion irradiation

Impacts of ions can do much larger modifications to graphene lattice than what is possible with electrons. This is mainly because of two major differences between electron and ion irradiation. Firstly, ions are much more massive than electrons, which allows for larger momentum transfer. Also, the space angle available for scattering is not limited in the case of ions for the same reason. Secondly, by choosing very low irradiation energies, and carefully selecting the ion species used in the process, it is possible to alter the local chemistry via introducing impurities. Obviously, electron irradiation can never alter the chemistry of a target system in this way.

Ion irradiation is an attractive method for a systematic study of the role of disorder on the properties of a material, because irradiation doses and hence the amount of disorder can be easily controlled. A two-dimensional target material brings in an additional advantage; very few (if any) ions will get

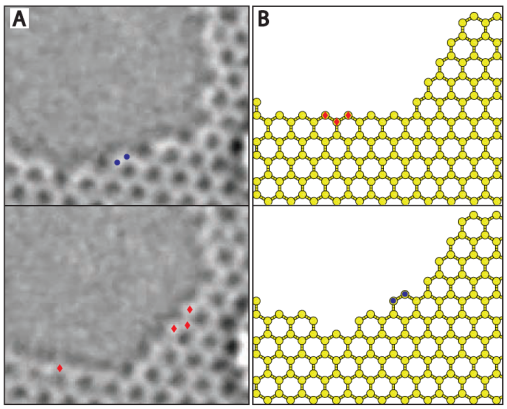

Figure 4: Edge reconfiguration. (A) Conversion of an armchair edge (top) to a zigzag edge (bottom). The two atoms marked as blue dots in the upper frame are gone in the lower frame, where four new carbon atoms are indicated as red diamonds. The 7-hexagon armchair edge is transformed into a 9-hexagon zigzag edge with a 60° turn. The transformation occurs due to migration of atoms along the edge. (B) Similar behavior is observed in the kinetic Monte Carlo simulation of hole growth, where three zigzag atoms (red diamonds, top) disappear and two armchair atoms (blue dots, bottom) appear. From Ref. [15]

trapped in the target material if this is intentionally avoided by selecting a high enough irradiation energy (above 100 eV). Already quite a few experiments on ion irradiation of graphene have been carried out. [19–22;29–32] To estimate the ion-irradiation–induced disorder in graphene, Raman spectroscopy [20;22], atomic force microscopy [21;22], local mobility measurements [29] and atomic resolution scanning tunneling microscopy [19] have been used, as described below.

2.3 Experimental identification of irradiation-induced defects

There are several experimental techniques which can be used to detect defects in carbon nanostructures in general and specifically in graphene. These techniques include scanning tunneling microscopy (STM) [19;33] and TEM (as explained above), which can be combined with transport measurements, micro Raman [20] and other spectroscopic techniques to get the signal from specific regions of the sample. Since the defects introduced with an electron beam in a TEM are typically directly analysed from the produced TEM images, the main

focus here is on defects produced via ion irradiation.

In Fig. 5, an example of an STM measurement of a defected area on graphite surface (*i.e.* top-most graphene layer of graphite) after Ar^+ irradiation is shown. Panel (a) displays four mono-vacancies (one missing atom) which each introduce a triangle shaped signal in spatial variation of the tunneling current. Local density of states [Fig. 5(d)] displays a peak density for a vacancy at the Fermi level indicating a flat defect state in the electronic band structure. Similar measurements, also with Ar^+ ions, have been carried out for graphene.[19] In these measurements, the defects were found to induce disorder in the hopping amplitudes in addition to acting as scattering centers for electrons. The most important consequence of the disorder is the substantial reduction in the Fermi velocity, revealed by bias-dependent imaging of electron-density oscillations near defect sites, unlike the sharp peak at the Fermi level for a mono-vacancy [Fig. 5(d)]. In the experiment reported in Ref.[19], the atomic structure of the defects was not identified. The observed hillocks in the STM images may have originated not only from defects in graphene, but also from defects in the substrate under graphene. Moreover, most defects were likely rather produced by atoms sputtered from the substrate rather than from the initial impacts by Ar^+ ions because the defect density appears higher than what would be expected from the irradiation dose (5×10^{11} ions/cm^2).

Another commonly used technique for estimating defect concentration of carbon nanostructures is Raman spectroscopy.[34;35] It should be pointed out that this technique can hardly be used to detect individual defects, as it provides information averaged over the finite laser spot area (typically hundreds of nm). In Fig. 6, the measured Raman spectra are shown for a graphene sheet irradiated with 500 eV Ne ions on top of a SiO_2 substrate.[20] The increase in the D band is an indication of the appearing defects, when compared to the pristine structure. Defect scattering was found to give a conductivity proportional to charge carrier density, with mobility decreasing as the inverse of the ion dose. Defected graphene was appeared to be insulating at low temperatures. The

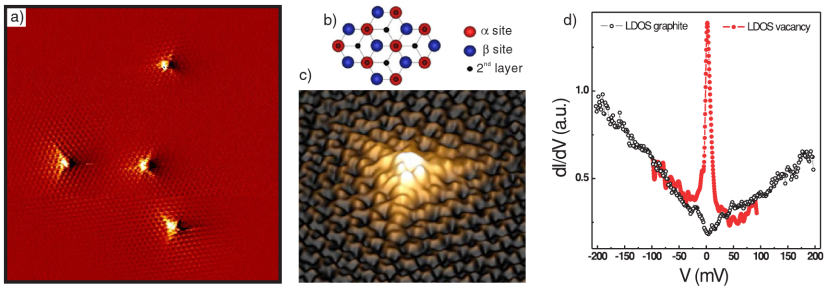

Figure 5: (a) 17×17 nm^2 STM topography, measured at 6 K, showing the graphite surface after the Ar^+ ion irradiation. Single vacancies occupy both α and β sites of the graphite honeycomb lattice. Sample bias: +270 mV, tunneling current: 1 nA. (b) Schematic diagram of the graphite structure. (c) 3D view of a single isolated vacancy. Sample bias: +150 mV, tunneling current: 0.5 nA. (d) STS measurements of the LDOS induced by single vacancy and of graphite. Black open circles correspond to dI/dV spectra measured on pristine graphite and red solid circles correspond to dI/dV spectra measured on top of the single vacancy, showing the appearance of a sharp resonance at E_F. dI/dV measurements were done consecutively at 6 K with the same microscopic tip. From Ref.[33]

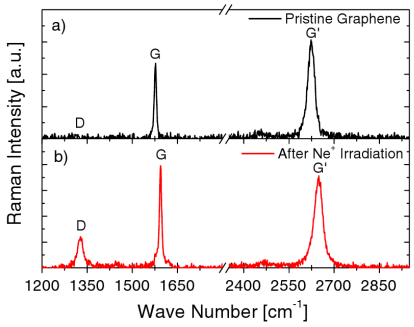

Figure 6: Raman spectra (wavelength 633 nm) for (a) pristine graphene and (B) graphene irradiated by 500 eV Ne ions at a dose of 5×10^{12} ions/cm^2. Note increase of the intensity of the D band associated with defects. From Ref.[20]

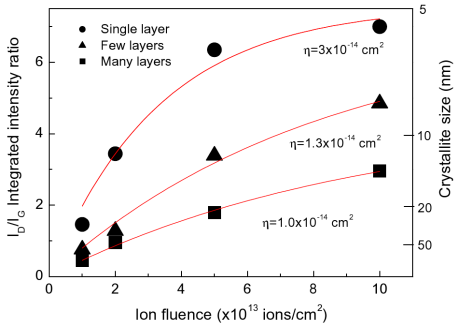

Figure 7: Ratio of the D peak and G peak intensities (I_D/I_G) as a function of the ion fluence ν for a mono-layer, a bi-layer and a multi-layer of graphene. From Ref.[22]

results were explained by ion-irradiation–induced localzied defect states in the electronic band structure. Although a comprehensive data set was produced on the effects of disorder on electronic transport in graphene, the microscopic nature of the produced defects in the reported experiments remain a mystery.

In another recent study,[22] a combination of atomic force microscopy (AFM) and Raman spectroscopy was used to assess the effects of a substrate layer and graphene on defect production. 500 keV carbon irradiation of mono-layer, bi-layer and multi-layer graphene on a SiO_2 substrate was carried out. At such high energies, electronic stopping dominates as the energy transfer method over nuclear stopping, which governs the process at lower energies. The ratio between the D peak and the G peak in mono-layer graphene was found to be higher than that for bi-layer or multi-layer structures (Fig. 7). This indicates a higher amount of disorder in the mono-layer structure, and the importance of the environment (the substrate) on defect production rate. AFM results also demonstrated that at fluences higher than 5×10^{13} cm^{-2} the morphology of mono-layers becomes fully conformed to that of the substrate, while graphene ripples are still present on bi-layers and multi-layers.

Graphene flakes have also been irradiated with 0.4–0.7 MeV protons on Si/SiO_2 substrates.[21] Again, the irradiated samples were investigated both by Raman spectroscopy and AFM. No increase in D band intensity was reported.

This is due to the fact that graphene becomes essentially transparent for protons with such high energies. AFM probing revelead bubble-like features which appeared at sample surface after the irradiation. This result was explained by agglomeration of gas molecules (most likely O_2 released from the SiO_2 substrate). This result also demonstrates the gas-holding ability of graphene – even after high energy proton irradiation.

Overall, despite the interesting insights into the influence of defects on graphene properties obtained from the first irradiation experiments on graphene, no microscopic picture of the damage production mechanism and defect types has been obtained experimentally. Even the interpretation of STM images is not straightforward, as various defects in graphitic systems can give rise to peaks in the local density of states near the Fermi energy.[36–38] Therefore, in order to understand the microscopic mechanisms which are active during the formation of these defects, atomistic simulations are needed. This is partly due to the much shorter times for defect production as compared to the exposure times in a TEM, and partly due to the fact that other techniques do not reveal the exact atomic configuration of the defected graphene.

3 Computational methods

Although the main focus of this Chapter is not on the computational methods used for graphene simulations but rather on giving an overview of the results obtained with them regarding defects in graphene, we feel that a short description of the methods is helpful for the reader at this point at least for the sake of defining the terms used later in this Chapter. For a more thorough discussion of the methods and their specific use in simulations of carbon systems we refer the reader to the recent review articles on the subject.[39;40] Below, we will briefly describe the different approximations used in simulating electron or ion irradiation of nanostructures. The methods are presented in the order of increasing accuracy (and thus transferability, but at the expense of increasing computational

cost). We omit here the statistical methods which can be employed to model events with macroscopic time scales (such as defect diffusion) because they can only be used to model the system after the actual irradiation event, and even then only when more accurate simulations have been first performed to map the possible events and relevant energetics. We stress, however, that these methods give useful insight when relating short-time-scale simulation results to the experiments, where annealing effects inevitably take place. An example of such a method for carbon nanostructures is the kinetic Monte Carlo model applied for defect migration on carbon nanotubes in Refs.[41;42]

Molecular dynamics (MD) simulations solve numerically the equations of motion for a set of interacting atoms with known initial coordinates $\mathbf{r}_i$ and velocities $\mathbf{v}_i$[43]. These methods have been of great use in modeling ion irradiation events in solids, and particularly in interpreting or predicting experimental results. Atomic interactions – both between two target atoms and between the ion and target atoms – can be described at different levels of sophistication: empirical potentials (EP), tight binding (TB) or density functional theory (DFT) models are typically employed. All these models can also be used in static calculations to understand energetics (and, in the case of quantum mechanical models, electronic properties) of native and irradiation-induced defects.

MD simulations of radiation effects are normally used to provide insight into qualitative mechanisms which cannot be directly assessed with experiments. However, several amendments are typically necessary when MD is used in out-of-equilibrium simulations. For radiation processes the most typically applied modifications are electronic stopping as a frictional force[44] (used with EP, can typically be omitted for carbon nanostructures where knock-on damage governs the ion irradiation process), realistic high energy repulsive interaction[45] (if all-electron DFT is not used) and adaptive time step (Δt), which both ensures that the Δt is not too large when energetic ions or atoms are present and that no computational time is wasted with a too short Δt when the system has cooled down.[44] It is also customary to apply one of several temperature control

methods (see *e.g.* Refs.[46–48]) to atoms at periodic boundaries to model heat dissipation in a much larger target structure. For a description of a typical simulation setup for irradiation simulations, we again refer to the recent review article on ion and electron irradiation effects in nanostructured materials.[40] If the reader is particularly interested in ion irradiation of graphene, we refer to the (so far) only MD study on the subject[18].

3.1 Empirical potentials (EP)

Empirical (or analytical) potentials are a set of equations which give the energy of the system as a function of the positions of the atoms. For each, a set of parameters is fitted to reproduce experimental results, or results obtained with methods of higher accuracy (typically DFT data). During the years, several interaction models have been developed for carbon. The most widely used one is the hydrocarbon potential by Brenner,[49] and its extensions.[50;51] For metals, models such as embedded atom method are widely employed.[52;53] For covalently bonded materials, bond order formalism, as implemented in Tersoff-like potentials (including the Brenner potential),[49;54;55] has proven to be a very good approximation. The major drawback of the empirical potentials is the fact that they have been fitted to a set of parameters which have been obtained for certain reference structures (typically in equilibrium). Thereby, one can never be sure how well these methods describe situations which have not been included in the fitting database. Nevertheless, empirical potentials have played an important role in increasing the understanding of ion irradiation in bulk materials, as well as in carbon nanostructures.

3.2 Tight binding (TB)

A step towards higher accuracy from EP is the tight binding (TB) model. TB is the simplest quantum mechanical method in atomistic simulations. In this approach the Schrödinger equation is solved for electrons moving in a field of atom cores, but the exact Hamiltonian is replaced by a parametrized matrix.

Parameters are most often obtained by fitting to the experimental or DFT data. Typically, atomic-like basis sets are used so that the Hamiltonian has the same symmetry properties as the atomic orbitals. A non-orthogonal self-consistent charge TB method[56;57] with parameters derived from DFT calculations (a second-order expansion of the Kohn-Sham total energy in DFT with respect to charge density fluctuations) has been successfully applied to model electron irradiation effects in covalently bonded materials such as carbon nanostructures.[58–60] DFT-based TB (DFTB) has also been used to model electron impacts in h-BN and BN nanotubes (along with carbon structures),[61] but, most likely due to ionic bonding, the BN results have caused much confusion when compared to the experimental results. Recent first principles calculations seem to resolve this issue.[62] For carbon materials this problem does not exist. Because fitting to the experimental data is avoided in DFTB, it has a much greater transferability than the conventional TB approaches. This makes it well suited for simulating irradiation events.

3.3 Density functional theory (DFT)

DFT approach (a good overview of the formalism and its implementation is offered in Ref.[63]) relies on two theorems by Hohenberg, Kohn and Sham. The theorems state that: (1) the ground state energy of a non-degenerate electronic state is a unique functional of its density; (2) this energy can be found by variation of the universal density functional with respect to the charge density. Hence, explicit treatment of the wavefunction of the system is not required. Instead, charge density is enough to find the ground state energy. This reduces the parameter space in the optimization from $3N$ (where N is the number of ions and electrons in the system) to 3 (spatial coordinates). However, the exact density functional is not known and must be approximated.

DFT and other quantum mechanical methods have a high accuracy, but they are computationally demanding. This limits the studied systems to a few hundred atoms and simulation times to picoseconds. Hence, most irradiation-

related problems are out of reach for these methods. DFT describes well the atomic structure of defects in many materials, and it has been successfully used for simulating behaviour of various defected systems. This makes DFT indispensable in understanding the structures after the irradiation event.

3.4 Time-dependent DFT (TD-DFT)

Conventional MD simulations are based on the Born-Oppenheimer approximation, which assumes that electrons are always in the ground state when the dynamics of the atoms is considered. For most cases, this is a valid assumption. However, when the velocities of the ions (atoms) approach the Fermi velocity v_F of the material (in graphene $v_F = 8 \times 10^5$ m/s, or $c/300$), this approximation becomes invalid. For ion irradiation, this limit would be reached at irradiation energy of 3 keV for proton as the projectile. In cases such as this, a combination of time dependent DFT and classical MD for ions[64;65] can be used to obtain microscopic insight into the interaction of energetic particles with target atoms, because the dynamics of the electronic system and that of the ions are treated on the same footing in real time. This method has also been applied in simulating proton collisions with carbon nanostructures[66].

3.5 Summary of the simulation methods

Due to the differences in the computational cost of the methods, they can be used to model events at different time scales and systems of different size. MD simulations within EP can be used to understand the microscopic processes during the ballistic phase of an irradiation event. In graphene, probability for creating collision cascades is drastically lowered from that of bulk structures because of the two-dimensional structure, but they nonetheless occur when the ion displaces a target atom with a trajectory in the direction of the graphene plane. In fact, the conventionally used binary collision model (in which the exact atomic structure of the target material is not explicitly described) fails in describing ion irradiation of graphene due to absence of collision cascades, as

described in Ref.[18] After the ballistic phase, MD can also describe the formation of heat spikes, their thermalization, formation of a sound/shock wave and how it spreads beyond the regime of the ballistic collisions. MD can also describe the nature of the defects produced. However, the major drawback of the MD method lies in the description of the defect structures and energetics. Quantum mechanical methods (DFTB, DFT) can provide a much more reliable picture of defect properties. As was mentioned above, these methods are limited by the system sizes and time scales they can handle. However, combining results of EP MD simulations and DFTB/DFT calculations makes it possible to reach accurate understanding on the actual defect production occurring during ion or electron irradiation of graphene and other carbon nanostructures.

4 Theoretical analysis of defects in graphene

More than 11% of the studies listed by ISI Web of Knowledge for a search with keyword "*graphene*" featured also words related to defects (*e.g.* "*defect*", "*dislocation*", "*vacancy*") (see Fig. 1). This gives an idea on the interest of the scientific community on defects in this material. As mentioned above, defects are interesting both by themselves because *e.g.* intrinsic defects appear in graphene used in experiments (especially in CVD grown graphene), and because they offer a possibility for tailoring the electric and magnetic properties of graphene and graphene-based electronic devices via controlled introduction of defects. Moreover, with respect to irradiation effects, it is clearly impossible to completely understand the irradiation response of any material without precise microscopic knowledge of the defect formation mechanisms.

The multitude of carbon allotropes with a variety of shapes and sizes is due to the ability of carbon to exist in various hybridizations. This also means that carbon networks can reorganize the atomic structure like no other material can do. New bonds restructure the lattice around defects by creating modified but coherent networks which retain many of the original properties of the structure.

This leads to a basically unlimited number of ways to accommodate extra and missing atoms in graphene. Carbon nanomaterials are also well known for their ability of self-healing during annealing.

In the following, we will turn our focus on both natural (intrinsic) defects and defects which can form due to electron or ion irradiation. Main stress will be on computational work in accordance with the topic of this Monograph. We will first discuss point defects, such as vacancies and carbon adatoms, including topological defects, *e.g.*, *Stone–Wales* defects. We will also address the evolution of point defects by briefly touching upon impurity atoms in graphene. The actual processes leading to the irradiation-induced defects are discussed later. We will also discuss line defects such as dislocation lines.

4.1 Point defects

Two of the most often considered defect structures in carbon nanomaterials are a mono-vacancy and a carbon adatom. Adatoms play the role of interstitials in graphene because there is not enough space for an interstitial to fit into the two-dimensional structure. In principle, an additional atom could fit into the open hollow of one of the hexagons, but this is energetically so much unfavored that it will never happen in practice. Another important example is the so called Stone-Wales defect formed by rotating a C–C bond.

4.1.1 Mono- and di-vacancies

When one carbon atom is simply removed from the graphene lattice, an immediate Jahn-Teller distortion[67–69] occurs to saturate the dangling bonds of two of the three under-coordinated carbon atoms [see Fig. 3(f) and Fig. 8]. This leads to a (5-9) defect structure in which one dangling bond remains in the middle of the 9-membered carbon ring. Contrary to metals, these reconstructions are a very prominent feature of vacancies in carbon nanomaterials, as demonstrated for example by high pressure created by removing atoms from carbon nanotubes[25] at high temperatures, so that the atomic bonds can efficiently

reconstruct. Formation energy for a mono-vacancy in graphene is about 7.5–7.7 eV as estimated with DFT calculations both within local density approximation (LDA)[68] and generalized gradient approximation (GGA).[70;71] Formation energy is here defined as

$$E_f = E_{\mathrm{d}}(N-n) + n\mu_{\mathrm{C}} - E(N), \tag{1}$$

where $E_{\mathrm{d}}(N-n)$ is the total energy of the defected structure composed from $N-n$ atoms, $\mu = E(N)/N$ is the chemical potential for carbon, $E(N)$ the total energy of the pristine system with N atoms and n the number of removed atoms when creating the vacancy. Note that E_f defines the energy difference between the defected system and the pristine one. It does not describe the energy needed to actually produce the defect – which is higher than E_f – because of a kinetic barrier in between the two states. Migration barrier for mono-vacancies has been estimated to be around 1.3–1.7 eV in graphene.[68]

After removing the under-coordinated atom of a mono-vacancy, a new bond is formed between the two new under-coordinated atoms, similar to what happens for a mono-vacancy (see Fig. 8). Thus we now get a (5-8-5) defect which is conventionally considered di-vacancy structure of carbon nanomaterials. Because of the saturation of all dangling bonds in the structure, we have again a sp^2-bonded carbon network (although with slightly distorted bond angles) where all atoms have three neighbors. In that way, graphene (and other sp^2-bonded carbon structures) are self-healing under irradiation. The saturation of the dangling bonds also leads to curious energetics of graphene vacancies since the di-vacancy formation energy is ca. 7.28 eV (or 3.64 eV/n where n is the number of missing atoms, as given by DFT GGA calculations with PBE parametrization[72;73]; earlier DFT LDA value is 8.7 eV[68]) *i.e.* sililart to that of a mono-vacancy. Di-vacancies have been thought to remain immobile in graphene due to a migration barrier of 7 eV.[68] However, taking into account the bond rotation process, they can actually travel under an electron beam. This matter

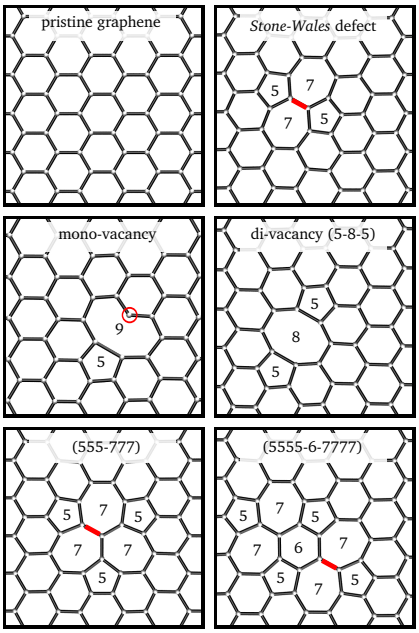

Figure 8: Different simple defect structures in graphene. *Stone–Wales* defect is obtained from pristine graphene by rotating the marked bond. In a similar manner, (555-777) is obtained from (5-8-5) and (5555-6-7777) from (555-777) by rotating the marked bonds. Also the under-coordinated atom of the mono-vacancy structure is marked.

is discussed in more detail below in the context of electron irradiation.

4.1.2 Multi-vacancies

As there is no way of removing an odd number of carbon atoms in such a way that the under-coordinated atoms could saturate the dangling bonds, it is clear that all energetically favored vacancy structures have an even number of missing atoms. This is similar to what was noticed for carbon nanotubes earlier.[74] The main difference between graphene and nanotubes is that in nanotubes a local diameter change assists in accommodating the locally lowered atomic density. A recent study[75] considered some simple multi-vacancy structures in graphene, and concluded that these defects could appear in nanoporous graphene with up to 1% concentration. However, the atoms in graphene can easily rearrange, which opens up the possibility for more complex polygon networks than what can happen in nanotubes or what was considered in Ref.[75] Nanoporous graphene has also been considered as a membrane for gas separation.[76]

An interesting example of complex polygon networks is the previously mentioned hæckelite structure[77] which consists of pentagons and heptagons arranged as a group of three pairs (555-777). When an individual (555-777) defect[78] is incorporated into graphene sheet (see Fig. 8), it is easy to notice that it accommodates two missing atoms. More interestingly, this structure can be obtained from the (5-8-5) defect by simply rotating one bond. As the local strain is reduced by transforming the octagon and tree hexagons to one pentagon and three heptagons, this defect has lower formation energy than the (5-8-5) di-vacancy [3.31 eV/n (DFT GGA); similar value has been reported in literature[78;79]]. Moreover, Lee *et al.* showed[80;81], using a TB model combined with MD, that a (5-8-5) divacancy can be formed from two separated vacancies via migration, and that the divacancy can transform to a (555-777) via bond rotation during the dynamical simulations. However, as the barrier for bond rotation is estimated to be at least 4-10 eV (depending on the local atomic configuration),[82] temperatures above 3000 K were needed to initiate

these transformations during times reachable in the simulations.

Jeong *et al.* did an extensive comparison of the energetics of dislocations and combinatorial (555-777) defect structures and noted that the (555-777) defects are energetically favored when eight or less atoms are missing, whereas dislocations would be preferred after this.[83] However, (555-777) and (5-8-5) are not the only possible di-vacancy structures which can occur in graphene. By rotating a nearby bond, a structure with four pentagons, four heptagons and one rotated hexagon (by 30°) in the middle of the grain boundary of alternating pentagons and heptagons is formed (5555-6-7777)[79] (see Fig. 8). Although this defect has a higher formation energy (ca. 3.35 eV/n) than the (555-777) defect, the energy difference is minor when compared to the (5-8-5) di-vacancy. In fact, in graphene nanoribbons (5555-6-7777) has been reported to have a lower formation energy than (555-777).[79]

It turns out that the (5555-6-7777) can be considered as the elementary multi-vacancy structure in graphene. The vacancy structure can be extended by adding these structures right next to each other so that pentagons of one overlap with the heptagons of the other. A rotated hexagon is obtained at each such polygon in the lattice. When more and more defects are added (and atoms thus removed), the structure starts to form a small misoriented grain in the graphene superlattice. For four and six missing atoms, it is possible to arrange these defects so that the formation energies (2.86 eV/n and 2.70 eV/n, as given by DFT GGA, respectively) are clearly below those for dislocations or combinatorial (555-777) defects. There is no reason why this could not be extended to larger multi-vacancy structures.

As a conclusion, there is a multitude of ways to arrange carbon atoms to form a polygon network to compensate for a certain number of missing atoms. However, the lowest energy multi-vacancy structures in graphene are formed by kernels of rotated hexagons which are accommodated to the zigzag edges of the surrounding graphene superlattice by a chain of alternating pentagons and heptagons. This notion is supported by the experimental results of extended

electron irradiation, which typically yields defects of this type (see Fig. 2).

4.1.3 Carbon adatoms

Carbon interstitials have played an important role in explaining radiation damage in graphite. These defects can easily appear after ion or electron impact, because of the empty space between the separate graphene layers. In principle, for each created mono-vacancy there exists an interstitial carbon atom somewhere else in graphite. Therefore, irradiating graphite will lead to formation of Frenkel pairs.[84] Adatoms also have an interesting role in self-healing of defected carbon nanotubes.[42] Again because of the two-dimensional structure, Frenkel pairs are far less frequently created in graphene, as displaced atoms are typically sputtered away (instead, vacancies will appear). As was mentioned above, no interstitial atoms in traditional sense exist in graphene. Instead, any additional atoms in graphene structures remain on top of the structure as adatoms.

Although creation of vacancies is less likely to produce adatoms in graphene than interstitial atoms in graphite, adatoms can still appear under certain experimental conditions. The reason for this is that graphene samples always contain carbon absorbates from which a TEM beam can sputter atoms which get trapped on the graphene mono-layers. When following the evolution of defect structures under TEM, one sometimes observes surprising increase in the number of carbon atoms at the defect, which is due to travelling carbon adatoms. The minimum energy configuration for carbon adatoms is the bridge structure in which the atom occupies a position on top of a carbon-carbon bond, as was shown recently.[85;86] The migration barrier in graphene has been estimated to be ca. 0.47 eV[85] (earlier estimates were even lower[87]), which means that they are highly mobile.

Carbon adatoms have also been suggested to play a role in catalyzing bond rotations[82] and self-healing processes,[88] and when joined as dimers to lead to *inverse Stone–Wales* defects and extended graphene bubble structures with locally introduced slight curvature.[89;90] However, bubbles of this kind remain to

be observed experimentally. Some interest in carbon adatoms on sp^2-bonded carbon structures has also resulted from the indications for introducing magnetism in these systems via additional atoms.[85;91]

4.1.4 Impurities on graphene

Impurity atoms can hardly be considered referred to as *native* defects in graphene. However, we want to stress that a considerable body of research has been carried out on this topic. On one hand, metal atoms and clusters play a major role in the catalytic activity during growth of carbon nanomaterials, and on the other hand, they have a major influence on the properties of these structures.[26] The chemisorbed adatoms on graphene either position themselves on top of a hexagon, on top of a carbon bond (e-type) or on top of a carbon atom (s-type).[92] Adatoms have been widely discussed in the context of magnetism (see *e.g.* Refs.[93–95]), but this has been far from the only subject of adatom studies.[93;94;96–104]

In addition to metal atoms, since B and N are the natural dopants in carbon systems, much interest has emerged on doping carbon nanomaterials with boron and nitrogen. For example, MD simulations[9;10] have shown that it is possible to get up to 40% of the impinging ions into the substitutional position in carbon nanotubes by selecting the irradiation energy appropriately. Later experiments confirmed that N irradiation of nanotubes indeed leads to substitutional doping.[11;12] Although the mentioned studies were made with carbon nanotubes, there is no fundamental physical reason why this would not work for graphene. Furthermore, due to the lack of curvature, one can expect even higher substitution probabilities for graphene than what was found for nanotubes.

Another topic which has gathered much attention regarding carbon nanomaterials is their ability to bind hydrogen in order to use them in hydrogen storage applications, to solve yet another problem which humankind is facing at the moment. So, perhaps ironically, carbon nanomaterials are considered to be a part of the solution for putting forward so-called *carbon-free technology*,

in which the energy production is no more based on fossil fuels. Since also this topic is beyond native defects and only remotely related to radiation damage in graphene, we simply list here in an exemplary way a few recent studies touching upon the subject (see *e.g.* Refs.[96;99;105–107]). Some work has also been done on hydrogen-related defects and their properties.[108–110]

4.1.5 Topological defects

So-called *Stone–Wales* defect[111] is probably the most famous defect in carbon nanostructures (see Fig. 8). It can be formed by selecting one bond in the hexagonal lattice and rotating it by 90° to transform four hexagons to two pentagons and two heptagons (5-7-5-7). Thus, the system is still composed of the "correct" number of atoms, but the atoms are arranged in a "wrong" way, so that we deal with topological disorder.

The formation of the SW defect is assisted by local curvature so that the formation energies are lower in fullerenes and carbon nanotubes than in graphene.[112–114] It is believed that the graphene sheet with a SW defects remains flat, although a recent study[115] utilizing highly accurate quantum mechanical calculations suggested that the formation of the defect could introduce a slight curvature in the lattice. The *Stone–Wales* defects have also been observed during TEM experiments [see Fig. 3(c)]. Although it has the lowest formation energy of any defects in carbon nanostructures ($E_f \approx 5.8$ eV in graphene according to quantum Monte Carlo calculations;[115] DFT GGA value is close to 4.6 eV), it is so high that room temperature equilibrium concentration should be too low to explain the frequent observations. As explained below, these defects are actually introduced during the observation under a TEM at acceleration voltages starting from ca. 80 kV via knock-on collisions between an electron and a single target atom.

In general, bond rotation is the other important way for altering graphene morphology in addition to removing atoms. Since bond rotations can change the hexagonal structure into a network of alternating pentagons, hexagons and

heptagons (or even tetragons and octagons although they have been much less frequently considered), this allows for a way to drastically change the local atomic structure but retaining the sp^2 bonding and thus flat – or almost flat – carbon membrane.

4.2 One-dimensional defects: Dislocations and grain boundaries

A glide dislocation monopole in graphene is formed by a pentagon-heptagon pair so that the shortest possible dislocation involves either a *Stone–Wales* defect or a *inverse Stone–Wales* defect, as shown in Ref.[89] Dislocations of different lengths – involving different numbers of missing atoms – are illustrated in Fig. 9. In their study,[83] Jeong and co-workers showed that dislocations are energetically favored over so-called hæckelite structures[77;80;81] when each structure has the same number of missing atoms ($N > 8$), as mentioned above in the context of multivacancy structures. In addition to accommodating missing atoms, extended dislocation structures serve as grain boundaries when they occur between two graphene grains with differing orientations.

A set of advanced ways of organizing the dislocation monopoles in a graphene superlattice was recently considered by Yazyev and Louie.[116] They developed a systematic approach for constructing atomic structures of topological defects in graphene, and were able to find grain boundary structures which exhibit extremely low formation energies (see Fig. 10 for example structures). The authors note that none of the considered atomic arrangements exhibited either electronic states at the Fermi level or magnetic moments.

With respect to the atomic configurations, one must keep in mind that in reality there are several other issues which play a role in determining the actual grain boundaries in addition to equilibrium thermodynamics of graphene. For example, when graphene is grown on a nickel substrate, the missmatch between graphene lattice and the underlaying Ni(111) surface leads to the formation of a grain boundary consisting of alternating sets of octagons and pentagon pairs

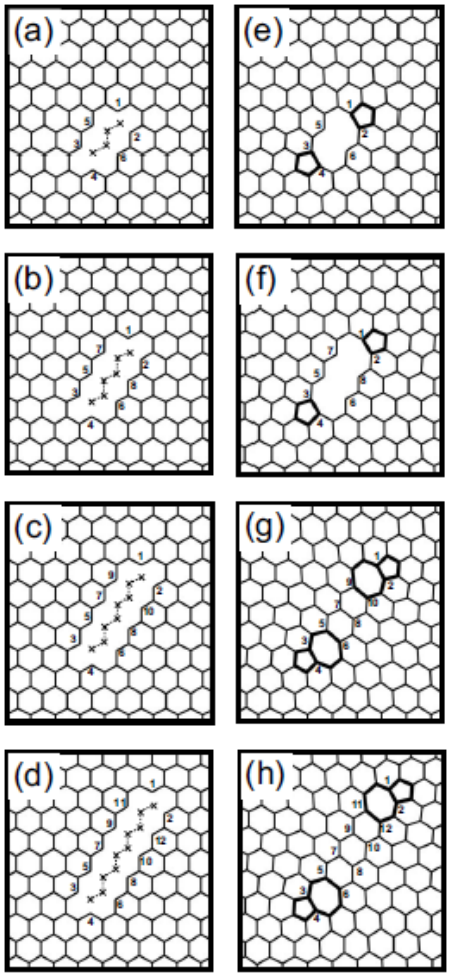

Figure 9: The initial geometries [(a)-(d)] and the relaxed geometries [(e)-(h)] of graphenes containing four [(a) and (e)], six [(b) and (f)], eight [(c) and (g)], and ten [(d) and (h)] vacancy units. Crosses and dashed lines in (a)-(d) indicate the positions of carbon vacancies and zigzag chains of carbon vacancies, respectively. The bold lines in (e)-(h) indicate pentagon and heptagon rings formed by the structural relaxation. From Ref.[83].

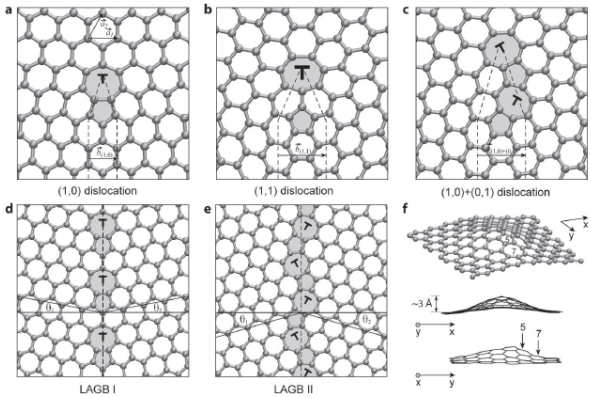

Figure 10: (a-c) Atomic structures of (1,0) and (1,1) dislocations, and a (1,0)+(0,1) dislocation pair, respectively. The dashed lines delimit the introduced semi-infinite strips of graphene originating at the dislocation core. Non-6-membered rings are shaded. (d,e) Atomic structures of the $\theta = 21.8°$ (LAGB I) and the $\theta = 32.2°$ (LAGB II) symmetric large-angle grain boundaries, respectively. The dashed lines show the boundary lines and the solid lines definite angles θ_1 and θ_2. (f) Buckling of the graphene layer due the presence of a (1,0) dislocation. From Ref. [116]

(see Fig. 11) [17]. Another way of obtaining this structure would be to align di-vacancies in graphene to the zigzag orientation. In contrast to the above-mentioned grain boundaries, this atomic arrangement was reported to display occupied electronic states at the Fermi level and thus to have metallic nature.

5 Irradiation-induced defects

All the discussed defects can be produced, at least in principle, by electron or ion irradiation of graphene. In order to fully understand why particular defects are more commonly encountered in the experiments, it is not sufficient to simply study the structure and energetics of the defects, but also the microscopic effects responsible for their production must be known.

5.1 Electron beam–driven morphological changes

The most accurate methods suitable for modeling electron beam damage in solids (DFT, TDDFT) cannot explicitly describe collisions of energetic electrons

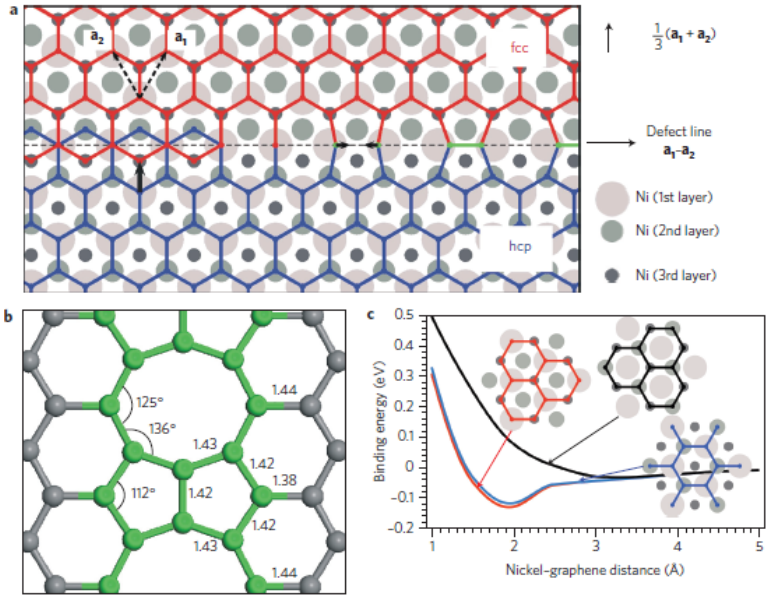

Figure 11: Structural model and schematic formation of an extended one-dimensional defect in graphene. Two graphene half-lattices, with unit cell vectors $\mathbf{a}_1$ and $\mathbf{a}_2$ (shown as dashed arrows), are translated by a fractional unit cell vector $1/3(\mathbf{a}_1 + \mathbf{a}_2)$, indicated by the vertical vector (solid arrow) (a). The two half-lattices can be joined along the $\mathbf{a}_1 - \mathbf{a}_2$ direction, indicated by the horizontal vector, without any unsaturated dangling bonds, by restructuring the graphene lattice. The domain boundary can be constructed as shown, by joining two carbon atoms, indicated by the two arrows, along the domain boundary line. This reconstructed domain boundary forms a periodic structure consisting of octagonal and pentagonal carbon rings. The underlying Ni(111) structure illustrates how the extended defect is formed by anchoring two graphene sheets to a Ni(111) substrate at slightly different adsorption sites. If one graphene domain has every second carbon atom located over a fcc-hollow site (red) and the other domain over a hcp-hollow site (blue), then the two domains are translated by $1/3(\mathbf{a}_1 + \mathbf{a}_2)$ relative to one another. The calculated adsorption energies for these two domains are very similar, but both are lower in energy than a third possible adsorption configuration with all carbon atoms on hollow sites, as shown in c. The DFT relaxed geometry of the defect structure, including bond lengths (in Å) and bond angles, is shown in b. From Ref. [17]

and ions in a solid. However, the damage created by energetic electrons can still be computed. Instead of launching an electron towards the structure in question, we can limit ourselves to studying what happens *after the fact*, *i.e.*, after the electron-ion collision has happened. To model the processes occurring in a TEM, it is sufficient to know the acceleration voltage used in the experiment. Then it can be relativistically calculated how much momentum (and thus kinetic energy) an electron can transfer (as a maximum) to a target atom:[23]

$$T_{\max} = \frac{2ME(E + 2mc^2)}{(m + M)^2c^2 + 2ME}, \tag{2}$$

where M is the mass of the target ion and m that of an electron, E the energy of the relativistic electron, and c the speed of light. If we now assign this kinetic energy to a certain target atom and follow the time evolution of the system, we can understand how certain TEM conditions will alter the morphology of the target material. However, in order to understand all events which can occur, one obviously must also consider energy transfer below the maximum ($T < T_{\max}$), and at all possible scattering angles.

The most important parameter is the displacement threshold T_d, which denotes the limiting kinetic energy above which the target atom will be displaced from its initial position. In pristine graphene this leads to a production of a single vacancy. In the case of a pre-existing vacancy, an additional atom will be sputtered. A thorough study was recently carried out within the DFTB approach by Zobelli and co-workers[61] in which T_d was calculated as a function of the scattering angle in carbon and BN nanotubes as well as in graphene (see Fig. 12; note the different notation for kinetic energy) and hexagonal BN mono-layers. Although their results for BN have caused some confusion in the interpretation of later experiments[117;118] it was still possible to explain the experimental results for the lowest energies used. Later DFT calculations[62] showed that indeed the displacement thresholds were underestimated, probably because of problems in describing the charge transfer in BN systems within

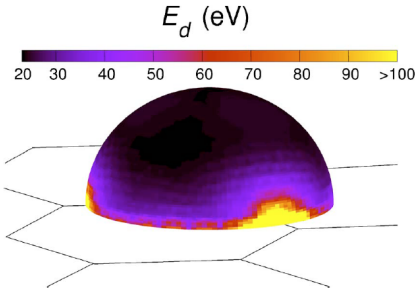

Figure 12: Three-dimensional representation of the map of the emission threshold function $E_d(\delta, \gamma)$ for a carbon atom in a graphitic layer as a function of the spherical coordinates δ and γ. The color scale indicates the emission energy values from 20 eV to more than 100 eV. The sphere indicates the emission direction for the ejected carbon atom. The sphere is centered on the initial position of the targeted C atom. From Ref.[61]

the DFTB model. In general, as discussed in Ref.[61], the theoretical T_d values can be expected to be 10–20% higher than the experimental ones, because only the ground-state dynamics is considered in the calculations. The beam-induced excitations may reduce the bonding energy of the atoms in the lattice, thus reducing the threshold energy. However, as the effect is expected to be systematic, one can assume that the obtained thresholds are over-estimations, and simply correct for this effect by reducing the threshold value to match the reference experimental data.

In order to calculate the actual displacements occurring under the electron beam, one can use the equation for the displacement cross section for a target atom within the McKinley-Feshbach formalism for Coulomb scattering[119] as[23]

$$\begin{aligned}\sigma &= \frac{4Z^2E_{\mathrm{R}}^2}{m^2c^4}\pi a_0^2\left(\frac{1-\beta^2}{\beta^4}\right) \\ &\quad\times\left\{1+2\pi\alpha\beta\left(\frac{T_d}{T_{\max}}\right)^{1/2}\right. \\ &\quad-\frac{T_d}{T_{\max}}\left[1+2\pi\alpha\beta\right. \\ &\quad\left.\left.+\left(\beta^2+\pi\alpha\beta\right)\ln\left(\frac{T_{\max}}{T_d}\right)\right]\right\}, \end{aligned} \tag{3}$$

where Z is the atomic number of the target atom, E_{R} the Rydberg energy

(13.6 eV), a_0 the Bohr radius (5.3×10^{-11} m), $\beta = v/c$, and $\alpha = Z/137$. Displacement rate becomes thus

$$p = \sigma j, \tag{4}$$

where j is the beam current.

The McKinley-Feshbach formalism assumes a uniform displacement threshold distribution over the relevant space angles. Although this at first might seem an unappropriate approximation noting that the T_d values, as reported in Ref.[61], vary from close to 20 eV up to more than 100 eV (DFT GGA value is ca. 22.2 eV, or 17.8–20.0 eV with a 10–20% correction corresponding to an acceleration voltage of 89.5–99.6 kV), one must also remember that due to the mass difference between an electron and a carbon atom, the possible scattering angles are all close to the direction parallel to the eletron beam. Within these angles, as seen in Fig. 12, the variations in T_d are rather small, and thus applying the McKinley-Feshbach formalism is justified.

After introducing the McKinley-Feshbach formalism, we now apply it for estimating electron beam damage in solids. As mentioned, the typical view has been that T_d is sufficient to describe the process. If energies higher than T_d are considered, it is obvious that the displaced carbon atom can introduce more structural changes in graphene. This obviously requires that the displacement occurs in a direction along the graphene plane, as noticed by Yazyev *et al.* [84] For example, they observed formation of *Stone–Wales* defects when a carbon atom is displaced into some in-plane directions with $T > 30$ eV. This and another example of their findings are shown in Fig. 13. The remarkable reorganization ability of carbon when the local atomic structure is disturbed is evident from this figure.

However, the in-plane displacement with $T > T_d$ cannot account for the reorganization which has been observed in graphene under continuous bombardment with electrons, as shown in Fig. 2(b), because in a typical TEM

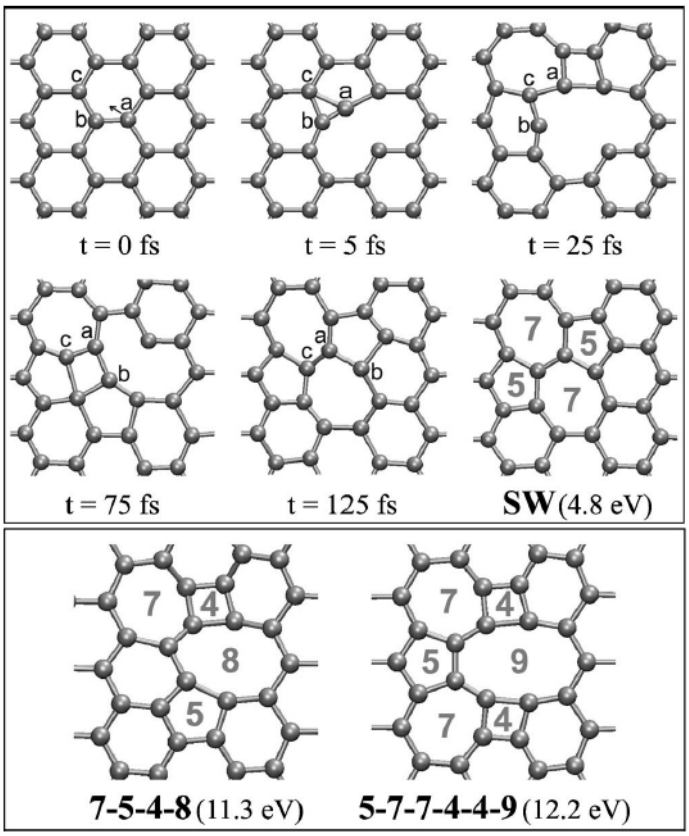

Figure 13: Top: The mechanism of formation of a Stone-Wales defect upon in-plane knock-on displacement. The carbon atoms involved in the rearrangement are marked with letters. Bottom: Atomic structures of 7-5-4-8 and 5-7-7-4-4-9 topological arabic numbers indicate non-hexagonal ring. From Ref. [84]

experiment graphene is set perpendicular to the electron beam for the best possible imaging conditions. Therefore, local heating effect of the electron beam has sometimes been thought to cause the reorganization events, as displayed in the high temperature simulations by Lee *et al.* [80;81]. This explanation fails for two reasons: (1) graphene is an excellent heat conductor, which means that any produced heat would be quickly dispersed to the whole structure and (2) single collisions between an electron and an ion would not bring about such heating as what would be required for providing enough energy for overcoming the 4–10 eV barriers for bond rotations.

The answer to this puzzle lies again in the extraordinary ability of carbon to reorganize when its atomic structure is perturbed. When simulations are carried out for momentum values (the momentum transferred from the electron to the ion) right below T_d at various space angles close to the electron beam direction, three outcomes are found. The most typical event is a failed ejection of an atom which leads back to pristine graphene. The second most typical event is the formation of a Frenkel pair where the atom can almost escape the graphene sheet, but still gets attached to it after it has moved away from its original position (Fig. 14). Due to low migration energy barrier, the atom can easily find its way back to recombine with the corresponding vacancy. The third possibility is a bond rotation, which occurs when the local atomic structure is perturbed, when the displaced atom either (1) is moved out from its original position, but doesn't have enough time to relax back before the atom returns (Fig. 15), or (2) circles around one of its neighbors due to the kick by the electron and drops back next to its original position thus forming the *Stone–Wales* defect (see Fig. 16).

These different processes have each a different kinetic energy threshold, similar to T_d, which defines the corresponding rate p at which they occur under a certain TEM beam. Therefore, by changing the acceleration voltage of the TEM, which defines the processes which can occur and corresponding p, one can select the ratios at which different processes occur. Below low-energy–limit, nothing

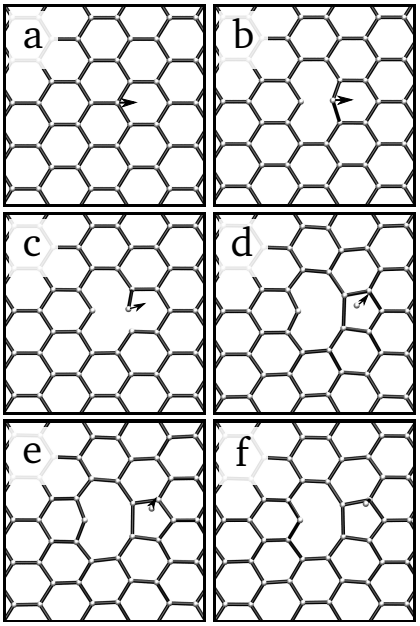

Figure 14: Formation of a Frenkel pair due to electron irradiation. As the atom remains close to the formed vacancy, it can easily migrate back and the defects can recombine. DFTB MD result.

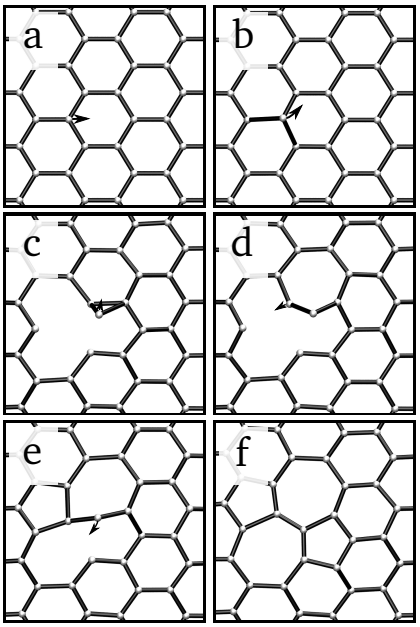

Figure 15: Formation of a *Stone–Wales* defect via the '*direct*' mechanism in which the displaced atom simply falls back to its original position, but pushes another atom during the process to cause a bond rotation. DFTB MD result.

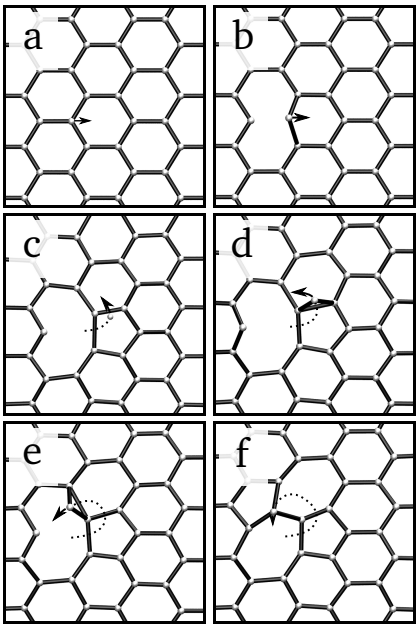

Figure 16: Formation of a *Stone–Wales* defect via the '*circle*' mechanism in which the displaced atom circles its neighbour and initiates the bond rotation. DFTB MD result.

happens to graphene, whereas at the other extreme (high energy and/or high dose) large holes are created. In between, the knock-on collision–driven bond rotations are active and play an important role in accommodating the locally lowered atomic density by producing complex polygon networks. The low T_d for displacing any dangling bond atoms in graphene (13.5 eV, or 10.8–12.2 eV with a 10–20% correction) is so low, that they are effectively ejected already at low acceleration voltages (50.0–62.8 kV), which means that under-coordinated carbon atoms are rarely observed in the complex polygon networks.

5.2 Ion irradiation–induced defect production

Since ions are much heavier than electrons and can thus transfer larger momentum to the target, ion irradiation has more profound effects on solids than electron irradiation. As mentioned before, the energy transfer to the electronic system of the target structure is not treated properly within the classical MD, but this is only relevant to simulations of graphene irradiation for high energies

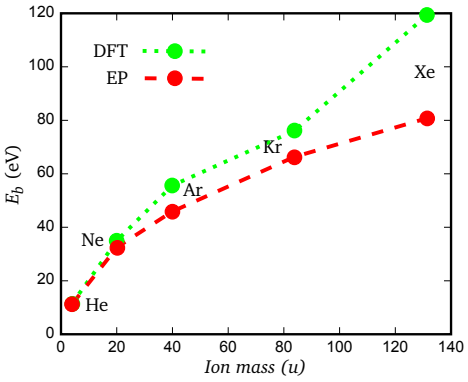

Figure 17: Comparison between DFT (GGA) and EP on the penetration barriers of various noble gas ions through a middle of a hexagon in graphene sheet as a function of the ion mass.

for the impinging ions. However, within the TDDFT formalism this effect is treated properly as demonstrated in Ref.[66]

In a recent study,[18] noble gas ion irradiation of graphene was simulated using the empirical potential by Brenner[49] to describe the carbon-carbon interaction amended with a correct description at short inter-atomic distances[45] and the universal repulsive potential for carbon-noble gas ion interactions.[45] To check for the validity of this method, graphene T_d was calculated by the Brenner interaction model (22.04 eV), and a surprisingly good agreement with DFT value (22.2 eV) was noted. Also the minimum kinetic energy needed for an Ar ion to cause an ejection of a carbon atom in graphene was calculated for both EP model and DFT GGA dynamical calculations. Obtained values were 32.33 eV and 32.74 eV, respectively. A good agreement was also noted for the penetration barrier for the noble gas ions through graphene. Again a good agreement between EP MD and DFT MD (see Fig. 17) was seen. From these comparisons it was concluded that the used EP method adequately describes the major features of the ion irradiation process of graphene.

From the results of the EP MD simulations, it was found that the produced defects can be grouped into following categories: mono-vacancies, di-vacancies, amorphous regions, Frenkel pairs and *Stone–Wales* defects. The last two contributed only a minor fraction to the bulk of the observed defects. Amorphiza-

tions included larger defected areas consisting of randomized polygon networks covering areas of up to 60 Å^2, but typically involving only one or two ejected carbon atoms. Any defects more complex than di-vacancies created in graphene are due to secondary recoils of a displaced carbon atom in the target plane.

Overall, the general trends for defect production in graphene under ion irradiation are as follow. If scattering angle for the carbon atom is close to the initial velocity of the ion, a mono-vacancy is produced [Fig. 18(a-d)] unless the ion hits right in the middle of a carbon-carbon bond and has such a velocity that the collision cross section between the ion and the two closest atoms is large enough to sputter both atoms and create a di-vacancy [Fig. 18(e-h)]. Otherwise, if a carbon atom is ejected, depending on the exact scattering angle and transferred momentum, the carbon atom can initiate ejection of another carbon atom [Fig. 18(i-l)] or a larger in-plane collision cascade which will lead to an amorphization event [Fig. 18(m-p)]. An in-plane collision will only occur at high irradiation energies, because it requires that the target atom is essentially immobile during the time it interacts with the ion; symmetric interaction with respect to the graphene plane will result in a displacement in direction perpendicular to the velocity of the ion.

Probabilities for producing various defects are presented for all considered ions as functions of irradiation energy in Fig. 19 along with a schematic illustration of the simulation setup and examples of the defect structures. By carefully selecting ion species and energy, it is possible to select such parameters from the data that for example 50% mono-vacancies and 50% di-vacancies will be produced with no additional defects. Varying this ratio, it is possible to study the effects these defects have on the electronic properties of graphene. One interesting aspect is the fact that when the energy is increased, for example for a Xe ion, the total defected area will be smaller than what would be procuded at lower energies with the same irradiation dose (for 2 MeV Xe the defected area becomes 30% of that of energies close to 0.5 keV). This opens up the possibility of using graphene in ion beam analysis methods as a membrane for irradiating

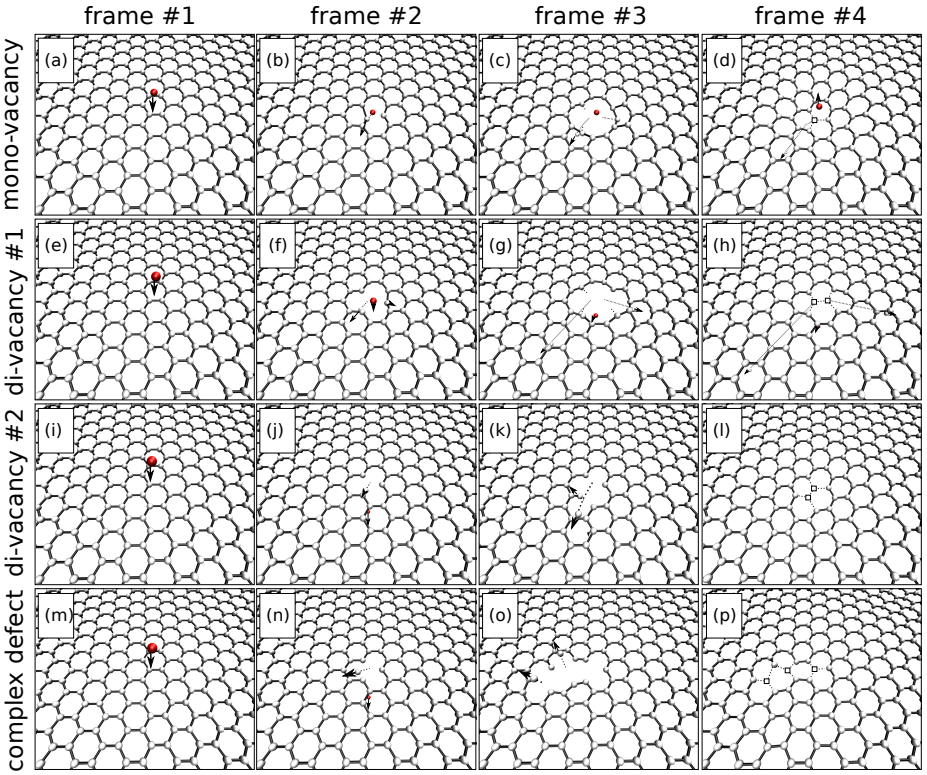

Figure 18: Defect creation processes during an ion irradiation event. Monovacancy is always produced by a direct knock-on displacement by the incoming ion (a-d). For di-vacancies, two formation mechanisms exist: direct displacement of both two atoms by low-energy ions (e-h) and higher-energy in-plane displacement of one atom which knocks out the second atom (i-l). All higher order defects are created by the in-plane displacements as shown in the example of a complex defect (m-p). Missing atoms are marked with squares in the last frame for each defect. Note that the lattice reconstructions have not had enough time to occur in these snapshots (and do not customarily appear in EP simulations, which needs to be taken into account when analysing the EP MD results).

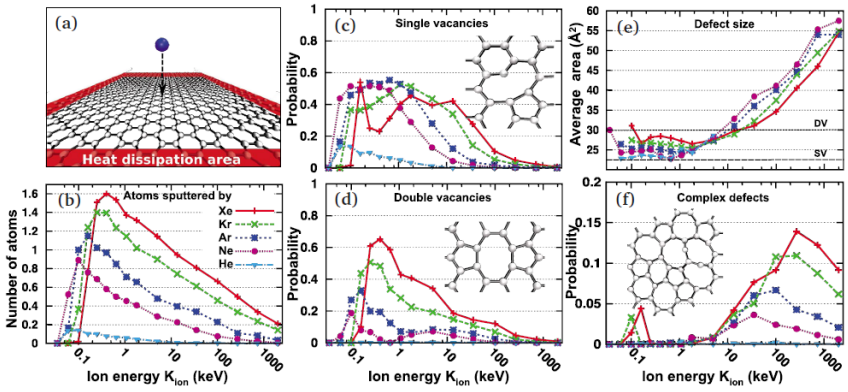

Figure 19: Production of defects in graphene under ion irradiation as revealed by EP MD. (a) Simulation setup. (b) Number of sputtered atoms per ion impact as a function of ion energy. [(c) and (d)] Probability for single and double vacancy formation as a function of ion energy. The insets show the atomic structures of the reconstructed vacancies. (e) Average area covered by a single defect (when formed) – typically still an sp^2-bonded network of carbon atoms. The areas corresponding to a SV and DV are marked. (f) Probability for creating defects other than SV/DV (except FP/SW), see the inset for an example. From Ref. [18].

volatile targets or targets which can not be put into a vacuum chamber (like pieces of art or living cells), especially when high energy ions can be used. Also, since the mono-vacancies dominate at the lower energies, where also the total damaged area is larger, it is evident that energies close to the mono-vacancy production maximum would be ideal for instance for cutting graphene with a focused ion beam (FIB).

The above results were obtained for ions oriented perpendicular to the graphene sheet. An additional parameter to control the defect production is the irradiation angle, bringing the number of parameters to three (ion mass m, energy K_{ion} and angle ψ). By varying the angle, one can shift the energies both at which the penetration of the ion through the graphene sheet occurs and when graphene becomes transparent for the ions (Fig. 20). The angle variation gives also some control on the defect types which will be created since by tilting graphene the projected atomic density under irradiation increases.

Clearly, the defect production in graphene under ion irradiation is a rather complex problem even for the non-bonding noble gases. As was shown above,

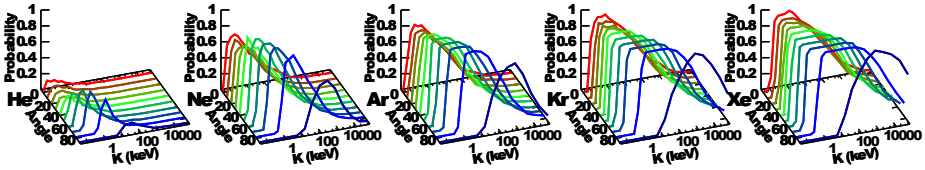

Figure 20: Defect creation probability of graphene under ion irradiation as a function of both irradiation angle ψ and energy K. Image courtesy of Ossi Lehtinen, University of Helsinki, Finland.

atomistic simulations will provide such insight into the relevant processes which can not be obtained using any current experimental methods. However, much of the work still remains to be done on this matter. Especially determining the conditions at which ion irradiation can be used to dope graphene with various elements such as boron, nitrogen or magnetic metals will be crucial if this method will be used in nanoengineering graphene with impurity atoms.

6 Conclusions and outlook

Understanding the structure and energetics of native defects in graphene is crucial since they may govern the electronic properties of the material. Especially CVD-grown graphene is known to contain a large number of dislocations and grain boundaries. In addition to pre-existing defects, some defects will inevitably be produced during the preparation of the material for applications. Moreover, defects can also be introduced deliberately into the structure in order to modify or study the properties of the system. Although the history of radiation damage studies in graphitic materials dates back to the past–World-War-II era, many of the microscopic processes which occur during the radiation process have remained unknown, especially in the context of mono-layer graphene, which became available for experiments only in the middle of the last decade (2004).

Effects of continued electron irradiation can be considered as collective sampling of separate elastic collisions between an electron and a target atom, each of which – when having any effect – will either (1) eject the atom, (2) create a

Frenkel pair where the displaced atom remains in the system as an adatom on graphene and can easily migrate back, or (3) cause a bond rotation. The actual rates for each of the events depends on the acceleration voltage *i.e.* kinetic energy of the electrons, and can be estimated within the McKinley-Feshbach formalism for Coulomb scattering. At the low energy limit, electron irradiation has no effect on graphene, whereas at the high energy/high dose limit atoms are simply sputtered. Curiously, in between these two extremes, graphene can accommodate the loss of atoms by reorganizing to form a complicated network of non-hexagonal rings via bond rotations.

Ion irradiation has a much stronger effect on graphene because of the larger momentum transfer between the ion and a target atom. When the transferred energy exceeds the displacement treshold, and the scattering angle of the target atom is close to the initial velocity of the ion, a mono-vacancy is always produced. When an ion hits in between two carbon atoms, which are nearest neighbours, and with a sufficient collision cross-section, a di-vacancy is directly produced. All other defects, and in fact also some di-vacancies, are created via secondary processes which are initiated by an in-plane displacement of the carbon atom. These only occur at high irradiation energies.

Atomistic simulations are the only way for obtaining detailed knowledge on microscopic events occurring during a radiation process of graphene. As graphene is the ultimately thin membrane with its thickness of only one atomic layer, the conventional knowledge of radiation damage in solids must be revised for this special case. Moreover, since carbon displays more flexibility in its ability to form molecules and rearrange bonds than any other element, many of the occurring processes are highly non-trivial. This opens possibilities to use atomistic simulations on radiation damage of carbon nanomaterials for designing experiments and methods which can be used for nanoengineering these exciting materials for possible uses in nanoelectronics, or perhaps as hydrogen storage.

To sum up, in this Chapter we presented an overview of the latest theoretical and experimental data on defects in graphene. We showed that atomistic com-

puter simulations carried out at different levels of sophistication ranging from empirical potential to first-principle techniques have proven to be an indispensable tool in the interpretation of the experimental results and in getting the microscopic understanding of the types of defects present in this material. We analyzed the structure of not only native but also irradiation-induced defects, and gave a detailed account of how the defects influence graphene properties. We also discussed at length the mechanisms of defect formation under ion and electron irradiation and pointed out new avenues for defect-mediated engineering of graphene-based structures and materials.

Acknowledgements

We wish to acknowledge Jannik Meyer and Ossi Lehtinen for contributing images and unpublished results to this Chapter. Our highest gratitude is due to Academy of Finland, which has provided us funding through several projects, and to Center for Scientific Computing, Espoo, Finland, for generous grants on computer time through the grand challenge program IECBN09.

References

[1] K. S. Novoselov, A. K. Geim, S. V. Morozov, D. Jiang, Y. Zhang, S. V. Dubonos, I. V. Grigorieva, and A. A. Firsov. Electric Field Effect in Atomically Thin Carbon Films. *Science*, 306(5696):666–669, 2004.

[2] P. R. Wallace. The band theory of graphite. *Phys. Rev.*, 71(9):622–634, May 1947.

[3] A. H. Castro Neto, F. Guinea, N. M. R. Peres, K. S. Novoselov, and A. K. Geim. The electronic properties of graphene. *Rev. Mod. Phys.*, 81(1):109–162, Jan 2009.

[4] Phaedon Avouris, Zhihong Chen, and Vasili Perebeinos. Carbon-based electronics. *Nat Nano*, 2(10):605–615, October 2007.

[5] Helin Cao, Qingkai Yu, Robert Colby, Deepak Pandey, C. S. Park, Jie Lian, Dmitry Zemlyanov, Isaac Childres, Vladimir Drachev, Eric A. Stach, Muhammad Hussain, Hao Li, Steven S. Pei, and Yong P. Chen. Large-scale graphitic thin films synthesized on ni and transferred to insulators: Structural and electronic properties. *J. Appl. Phys.*, 107(4):044310, 2010.

[6] Stanley B. Austerman and John E. Hove. Irradiation of graphite at liquid helium temperatures. *Phys. Rev.*, 100(4):1214–1215, Nov 1955.

[7] S. Iijima. Helical microtubules of graphitic carbon. *Nature*, 354:56–58, 1991.

[8] James W. Mayer and S. S. Lau. *Electronic Materials Science For Integrated Circuits in Si and GaAs.* MacMillan, New York, 1990.

[9] J. Kotakoski, A. V. Krasheninnikov, Yuchen Ma, A. S. Foster, K. Nordlund, and R. M. Nieminen. B and n ion implantation into carbon nanotubes: Insight from atomistic simulations. *Phys. Rev. B*, 71(20):205408, May 2005.

[10] J. Kotakoski, J.A.V. Pomoell, A.V. Krasheninnikov, and K. Nordlund. Irradiation-assisted substitution of carbon atoms with nitrogen and boron in single-walled carbon nanotubes. *Nucl. Instr. and Meth. in Phys. Res. B*, 228(1-4):31–36, 2005. Proceedings of the Seventh International Conference on Computer Simulation of Radiation Effects in Solids.

[11] C. Morant, J. Andrey, P. Prieto, D. Mendiola, J. M. Sanz, and E. Elizalde. Xps characterization of nitrogen-doped carbon nanotubes. *Phys. Stat. Sol.*, 203:1069–1075, 2006.

[12] F. Xu, M. Minniti, P. Barone, A. Sindona, A. Bonanno, and A. Oliva. Nitrogen doping of single walled carbon nanotubes by low energy ion implantation. *Carbon*, 46(11):1489–1496, 2008.

[13] A. Hashimoto, K. Suenaga, A. Gloter, K. Urita, and S. Iijima. Direct evidence for atomic defects in graphene layers. *Nature (London)*, 430:870, 2004.

[14] Jannik C. Meyer, C. Kisielowski, R. Erni, Marta D. Rossell, M. F. Crommie, and A. Zettl. Direct imaging of lattice atoms and topological defects in graphene membranes. *Nano Letters*, 8(11):3582–3586, November 2008.

[15] Caglar O. Girit, Jannik C. Meyer, Rolf Erni, Marta D. Rossell, C. Kisielowski, Li Yang, Cheol-Hwan Park, M. F. Crommie, Marvin L. Cohen, Steven G. Louie, and A. Zettl. Graphene at the Edge: Stability and Dynamics. *Science*, 323(5922):1705–1708, 2009.

[16] G. Gómez-Navarro, P. J. De Pablo, J. Gómez-Herrero, B. Biel, F. J. Garcia-Vidal, A. Rubio, and F. Flores. Tuning the conductance of single-walled carbon nanotubes by ion irradiation in the anderson localization regime. *Nat. Mater.*, 4:534, 2005.

[17] Jayeeta Lahiri, You Lin, Pinar Bozkurt, Ivan I. Oleynik, and Matthias Batzill. An extended defect in graphene as a metallic wire. *Nat Nano*, 5:326–329, 2010.

[18] O. Lehtinen, J. Kotakoski, A.V. Krasheninnikov, A. Tolvanen, K. Nordlund, and J. Keinonen. Effect of ion bombardment on a two-dimensional target: atomistic simulations of graphene irradiation. *Phys. Rev. B*, 81:153401, 2010.

[19] L. Tapasztó, G. Dobrik, P. Nemes-Incze, G. Vertesy, Ph. Lambin, and L. P. Biró. Tuning the electronic structure of graphene by ion irradiation. *Phys. Rev. B*, 78(23):233407, Dec 2008.

[20] Jian-Hao Chen, W. G. Cullen, C. Jang, M. S. Fuhrer, and E. D. Williams. Defect scattering in graphene. *Phys. Rev. Lett.*, 102(23):236805, 2009.

[21] E. Stolyarova, D. Stolyarov, K. Bolotin, S. Ryu, L. Liu, K. T. Rim, M. Klima, M. Hybertsen, I. Pogorelsky, I. Pavlishin, K. Kusche, J. Hone, P. Kim, H. L. Stormer, V. Yakimenko, and G. Flynn. Observation of graphene bubbles and effective mass transport under graphene films. *Nano Letters*, 9(1):332–337, 2009.

[22] Giuseppe Compagnini, Filippo Giannazzo, Sushant Sonde, Vito Raineri, and Emanuele Rimini. Ion irradiation and defect formation in single layer graphene. *Carbon*, 47(14):3201–3207, 2009.

[23] F. Banhart. Irradiation effects in carbon nanostructures. *Rep. Prog. Phys.*, 62:1181–1221, 1999.

[24] Mhairi H. Gass, Ursel Bangert, Andrew L. Bleloch, Peng Wang, Rahul R. Nair, and GeimA. K. Free-standing graphene at atomic resolution. *Nat Nano*, 3(11):676–681, November 2008.

[25] L. Sun, F. Banhart, A. V. Krasheninnikov, J. A. Rodríguez-Manzo, M. Terrones, and P. M. Ajayan. Carbon nanotubes as high-pressure cylinders and nanoextruders. *Science*, 312:1199, 2006.

[26] Litao Sun, Arkady V. Krasheninnikov, Tommy Ahlgren, Kai Nordlund, and Florian Banhart. Plastic deformation of single nanometer-sized crystals. *Phys. Rev. Lett.*, 101(15):156101, 2008.

[27] Chuanhong Jin, Haiping Lan, Lianmao Peng, Kazu Suenaga, and Sumio Iijima. Deriving carbon atomic chains from graphene. *Phys. Rev. Lett.*, 102(20):205501, 2009.

[28] Andrey Chuvilin, Jannik C Meyer, Gerardo Algara-Siller, and Ute Kaiser. From graphene constrictions to single carbon chains. *New J. Phys.*, 11(8):083019 (10pp), 2009.

[29] F. Giannazzo, S. Sonde, V. Raineri, and E. Rimini. Irradiation damage

in graphene on sio[sub 2] probed by local mobility measurements. *Appl. Phys. Lett.*, 95(26):263109, 2009.

[30] S. H. M. Jafri, K. Carva, E. Widenkvist, T. Blom, B. Sanyal, J. Fransson, O. Eriksson, U. Jansson, H. Grennberg, O. Karis, R. A. Quinlan, B. C. Holloway, and K. Leifer. Conductivity engineering of graphene by defect formation. *J. Phys. D: Appl. Phys.*, 43(4):045404, 2010.

[31] Ki-Jeong Kim, Hangil Lee, Junghun Choi, Hankoo Lee, Min Cherl Jung, H J Shin, T-H Kang, B Kim, and Sehun Kim. Surface property change of graphene using nitrogen ion. *J. Phys. Cond. Matt.*, 22(4):045005 (4pp), 2010.

[32] Kyu Won Lee, H. Kweon, J. J. Kweon, and Cheol Eui Lee. Electron spin resonance study of proton-irradiation-induced defects in graphite. *J. Appl. Phys.*, 107(4):044302, 2010.

[33] M. M. Ugeda, I. Brihuega, F. Guinea, and J. M. Gómez-Rodríguez. Missing atom as a source of carbon magnetism. *Phys. Rev. Lett.*, 104(9):096804, Mar 2010.

[34] A. C. Ferrari, J. C. Meyer, V. Scardaci, C. Casiraghi, M. Lazzeri, F. Mauri, S. Piscanec, D. Jiang, K. S. Novoselov, S. Roth, and A. K. Geim. Raman spectrum of graphene and graphene layers. *Phys. Rev. Lett.*, 97(18):187401, Oct 2006.

[35] Andrea C. Ferrari. Raman spectroscopy of graphene and graphite: Disorder, electron-phonon coupling, doping and nonadiabatic effects. *Solid State Communications*, 143(1-2):47–57, 2007. Exploring graphene - Recent research advances.

[36] Antti Tolvanen, Gilles Buchs, Pascal Ruffieux, Pierangelo Groning, Oliver Groning, and Arkady V. Krasheninnikov. Modifying the electronic structure of semiconducting single-walled carbon nanotubes by ar^+ ion irradiation. *Phys. Rev. B*, 79(12):125430, 2009.

[37] A. V. Krasheninnikov, K. Nordlund, M. Sirviö, E. Salonen, and J. Keinonen. Formation of ion irradiation-induced atomic-scale defects on walls of carbon nanotubes. *Phys. Rev. B*, 63:245405, 2001.

[38] A. V. Krasheninnikov. Predicted scanning microscopy images of carbon nanotubes with atomic vacancies. *Solid State Commun.*, 118:361–365, 2001.

[39] D. Tománek. Carbon-based nanotechnology on a super computer. *J. Phys. Condens. Matter*, 17:R413, 2005.

[40] A. V. Krasheninnikov and K. Nordlund. Ion and electron irradiation-induced effects in nanostructured materials. *J. Appl. Phys.*, 107(7):071301, 2010.

[41] J. Kotakoski, A. V. Krasheninnikov, and K. Nordlund. Kinetic Monte Carlo simulations of the response of carbon nanotubes to electron irradiation. *J. Comp. Theor. Nanosci.*, 4(6):1153–1159, Sep 2007.

[42] Yanjie Gan, J. Kotakoski, A. V. Krasheninnikov, K. Nordlund, and F. Banhart. The diffusion of carbon atoms inside carbon nanotubes. *New J. Phys.*, 10, Feb 15 2008.

[43] M. P. Allen and D. J. Tildesley. *Computer Simulation of Liquids*. Oxford University Press, Oxford, England, 1989.

[44] K. Nordlund, J. Keinonen, and A. Kuronen. Effect on the interatomic si-si-potential on vacancy production during ion implantation of si. *Physica Scripta*, T54:34–37, 1995.

[45] J. F. Ziegler, J. P. Biersack, and U. Littmark. *The Stopping and Range of Ions in Matter*. Pergamon, USA, 1985.

[46] H. J. C. Berendsen, J. P. M. Postma, W. F. van Gunsteren, A. DiNola, and J. R. Haak. Molecular dynamics with coupling to external bath. *J. Chem. Phys.*, 81(8):3684, 1984.

[47] S. Nose. A molecular-dynamics method for simulations in the canonical ensemble. *Mol. Phys.*, 52(2):255–268, 1984.

[48] S. Nose. A unified formulation of the constant temperature molecular-dynamics methods. *J. Chem. Phys.*, 81(1):511–519, 1984.

[49] D. W. Brenner. Empirical potential for hydrocarbons for use in simulating the chemical vapor deposition of diamond films. *Phys. Rev. B*, 42:9458–9471, 1990.

[50] S. J. Stuart, A. B. Tutein, and J. A. Harrison. A reactive potential for hydrocarbons with intermolecular interactions. *J. Chem. Phys.*, 112(14):6472–6486, 2000.

[51] D. W. Brenner, O. A. Shenderova, J. A. Harrison, S. J. Stuart, B. Ni, and S. B. Sinnott. A second-generation reactive empirical bond order (rebo) potential energy expression for hydrocarbons. *J.Phys.: Condens. Matter*, 14:783–802, 2002.

[52] M. S. Daw, S. M. Foiles, and M. I. Baskes. The embedded-atom-method: a review of theory and applications. *Mat. Sci. Rep.*, 9:251–287, 1993.

[53] C. I. Kelchner, D. M. Halstead, L. S. Perkins, N. M Wallace, and A. E. DePristo. Construction and evaluation of embedding functions. *Surf. Sci.*, 310:425–435, 1994.

[54] J. Tersoff. Empirical interatomic potential for carbon, with applications to amorphous carbon. *Phys. Rev. Lett.*, 61(25):2879, 1988.

[55] K. Albe, K. Nordlund, and R. S. Averback. Modeling the metal-semiconductor interaction: Analytical bond-order potential for platinum-carbon. *Phys. Rev. B*, 65(19):195124, May 2002.

[56] D. Porezag, Th. Frauenheim, Th. Köhler, G. Seifert, and R. Kaschner. Construction of tight-binding-like potentials on the basis of density-

functional theory: Application to carbon. *Phys. Rev. B*, 51(19):12947–12957, May 1995.

[57] M. Elstner, D. Porezag, G. Jungnickel, J. Elsner, M. Haugk, Th. Frauenheim, S. Suhai, and G. Seifert. Self-consistent-charge density-functional tight-binding method for simulations of complex materials properties. *Phys. Rev. B*, 58(11):7260–7268, Sep 1998.

[58] F. Banhart, J. X. Li, and A. V. Krasheninnikov. Carbon nanotubes under electron irradiation: Stability of the tubes and their action as pipes for atom transport. *Phys.Rev.B*, 71:241408(R), 2005.

[59] A. V. Krasheninnikov, F. Banhart, J. X. Li, A.S. Foster, and R.M. Nieminen. Stability of carbon nanotubes under electron irradiation: Role of tube diameter and chirality. *Phys. Rev. B*, 72:125428, 2005.

[60] T. Loponen, A. V. Krasheninnikov, M. Kaukonen, and R. M. Nieminen. Nitrogen-doped carbon nanotubes under electron irradiation simulated with a tight-binding model. *Phys. Rev. B*, 74(7):073409, Aug 2006.

[61] A. Zobelli, Gloter A., Ewels C. P., G. Seifert, and C. Colliex. Electron knock-on cross section of carbon and boron nitride nanotubes. *Phys. Rev. B*, 75:245402, 2007.

[62] J. Kotakoski, C. H. Jin, O. Lehtinen, K. Suenaga, and A. V. Krasheninnikov. Knock-on damage in hexagonal boron nitride monolayers. *Phys. Rev. Lett.*, 2010. submitted for publication.

[63] R. Martin. *Electronic structure*. Cambridge University Press, Cambridge, UK, 2004.

[64] Osamu Sugino and Yoshiyuki Miyamoto. Density-functional approach to electron dynamics: Stable simulation under a self-consistent field. *Phys. Rev. B*, 59(4):2579–2586, Jan 1999.

[65] Osamu Sugino and Yoshiyuki Miyamoto. Erratum: Density-functional approach to electron dynamics: Stable simulation under a self-consistent field [phys. rev. b 59, 2579 (1999)]. *Phys. Rev. B*, 66(8):089901, Aug 2002.

[66] A. V. Krasheninnikov, Y. Miyamoto, and D. Tomanek. Role of electronic excitations in ion collisions with carbon nanostructures. *Phys. Rev. Lett.*, 99:016104, 2007.

[67] R.H. Telling, C.P. Ewels, A.A. El-Barbary, and M.I. Heggie. Wigner defects bridge the graphite gap. *Nat. Mater.*, 2:333–337, 2003.

[68] A. A. El-Barbary, R. H. Telling, C. P. Ewels, M. I. Heggie, and P. R. Briddon. Structure and energetics of the vacancy in graphite. *Phys. Rev. B*, 68(14):144107, Oct 2003.

[69] P. O. Lehtinen, A. S. Foster, Y. Ma, A. V. Krasheninnikov, and R. M. Nieminen. Irradiation-induced magnetism in graphite: A density functional study. *Phys. Rev. Lett.*, 93:187202, 2004.

[70] L. Li, S. Reich, and J. Robertson. Defect energies of graphite: Density-functional calculations. *Phys. Rev. B*, 72(18):184109, Nov 2005.

[71] A. V. Krasheninnikov, P. O. Lehtinen, A. S. Foster, and R. M. Nieminen. Bending the rules: Contrasting vacancy energetics and migration in graphite and carbon nanotubes. *Chem. Phys. Lett.*, 418:132–136, 2006.

[72] J. P. Perdew, K. Burke, and M. Ernzerhof. Generalized gradient approximation made simple. *Phys. Rev. Lett.*, 77:3865, 1996.

[73] J. P. Perdew, K. Burke, and M. Ernzerhof. Erratum: Generalized gradient approximation made simple. *Phys. Rev. Lett.*, 78:1396, 1997.

[74] J. Kotakoski, A. V. Krasheninnikov, and K. Nordlund. Energetics, structure, and long-range interaction of vacancy-type defects in carbon nanotubes: Atomistic simulations. *Phys. Rev. B*, 74(24), Dec 2006.

[75] Johan M. Carlsson and Matthias Scheffler. Structural, electronic, and chemical properties of nanoporous carbon. *Phys. Rev. Lett.*, 96(4):046806, 2006.

[76] De en Jiang, Valentino R. Cooper, and Sheng Dai. Porous graphene as the ultimate membrane for gas separation. *Nano Letters*, pages 4019–4024, September 2009.

[77] H. Terrones, M. Terrones, E. Hernández, N. Grobert, J-C. Charlier, and P. M. Ajayan. New metallic allotropes of planar and tubular carbon. *Phys. Rev. Lett.*, 84(8):1716–1719, Feb 2000.

[78] Rodrigo G. Amorim, A. Fazzio, Alex Antonelli, Frederico D. Novaes, and Antonio J. R. da Silva. Divacancies in graphene and carbon nanotubes. *Nano Letters*, 7(8):2459–2462, August 2007.

[79] R. Y. Oeiras, F. M. Araujo-Moreira, and E. Z. da Silva. Defect-mediated half-metal behavior in zigzag graphene nanoribbons. *Phys. Rev. B*, 80(7):073405, 2009.

[80] G. D. Lee, C. Z. Wang, E. Yoon, N. M. Hwang, D. Y. Kim, and K. M. Ho. Diffusion, coalescence, and reconstruction of vacancy defects in graphene layers. *Phys. Rev. Lett.*, 95:205501, 2005.

[81] Gun-Do Lee, C. Z. Wang, Euijoon Yoon, Nong-Moon Hwang, and K. M. Ho. Vacancy defects and the formation of local haeckelite structures in graphene from tight-binding molecular dynamics. *Phys. Rev. B*, 74(24):245411, Dec 2006.

[82] C. P. Ewels, M. I. Heggie, and P. R. Briddon. Adatoms and nanoengineering of carbon. *Chem. Phys. Lett.*, 351:178–182, 2002.

[83] Byoung Wook Jeong, Jisoon Ihm, and Gun-Do Lee. Stability of dislocation defect with two pentagon-heptagon pairs in graphene. *Phys. Rev. B*, 78(16):165403, 2008.

[84] Oleg V. Yazyev, Ivano Tavernelli, Ursula Rothlisberger, and Lothar Helm. Early stages of radiation damage in graphite and carbon nanostructures: A first-principles molecular dynamics study. *Phys. Rev. B*, 75(11):115418, 2007.

[85] P. O. Lehtinen, A. S. Foster, A. Ayuela, A.V. Krasheninnikov, K. Nordlund, and R. M. Nieminen. Magnetic properties and diffusion of adatoms on a graphene sheet. *Phys. Rev. Lett.*, 91:017202, 2003.

[86] A. V. Krasheninnikov, K. Nordlund, Lehtinen P. O., A. S. Foster, A. Ayuela, and R. M. Nieminen. Adsorption and migration of carbon adatoms on carbon nanotubes: Density-functional *ab initio* and tight-binding studies. *Phys. Rev. B*, 69:073402, 2004.

[87] M. Heggie, B. R. Eggen, C. P. Ewels, P. Leary, S. Ali, G. Jungnickel, R. Jones, and P. R. Briddon. Ldf calculations of point defects in graphites and fullerenes. *Electrochem. Soc. Proc.*, 98:60, 1998.

[88] L. Tsetseris and S.T. Pantelides. Adatom complexes and self-healing mechanisms on graphene and single-wall carbon nanotubes. *Carbon*, 47(3):901–908, 2009.

[89] Mark T. Lusk, David T. Wu, and Lincoln D. Carr. Graphene nano-engineering and the inverse stone-thrower-wales defect. *Phys. Rev. B*, 81(15):155444, Apr 2010.

[90] Mark T. Lusk and L. D. Carr. Nanoengineering defect structures on graphene. *Phys. Rev. Lett.*, 100(17):175503, Apr 2008.

[91] Ranber Singh and Peter Kroll. Magnetism in graphene due to single-atom defects: dependence on the concentration and packing geometry of defects. *J. Phys. Cond. Matt.*, 21(19):196002, 2009.

[92] Vadim V. Cheianov, Olav Syljuasen, B. L. Altshuler, and Vladimir Fal'ko.

Ordered states of adatoms on graphene. *Phys. Rev. B*, 80(23):233409, 2009.

[93] Bruno Uchoa, Ling Yang, S.-W. Tsai, N. M. R. Peres, and A. H. Castro Neto. Theory of scanning tunneling spectroscopy of magnetic adatoms in graphene. *Phys. Rev. Lett.*, 103(20):206804, Nov 2009.

[94] Harman Johll, Hway Chuan Kang, and Eng Soon Tok. Density functional theory study of fe, co, and ni adatoms and dimers adsorbed on graphene. *Phys. Rev. B*, 79(24):245416, 2009.

[95] E. J. G. Santos, D. Sánchez-Portal, and A. Ayuela. Magnetism of substitutional co impurities in graphene: Realization of single π vacancies. *Phys. Rev. B*, 81(12):125433, Mar 2010.

[96] C. Ataca, E. Akturk, S. Ciraci, and H. Ustunel. High-capacity hydrogen storage by metallized graphene. *Appl. Phys. Lett.*, 93(4):043123, 2008.

[97] Kevin T. Chan, J. B. Neaton, and Marvin L. Cohen. First-principles study of metal adatom adsorption on graphene. *Phys. Rev. B*, 77(23):235430, 2008.

[98] A. H. Castro Neto and F. Guinea. Impurity-induced spin-orbit coupling in graphene. *Phys. Rev. Lett.*, 103(2):026804, Jul 2009.

[99] Woo Sik Kim, Sook Young Moon, Sin Young Bang, Bong Geun Choi, Heon Ham, Tohru Sekino, and Kwang Bo Shim. Fabrication of graphene layers from multiwalled carbon nanotubes using high dc pulse. *Appl. Phys. Lett.*, 95(8):083103, 2009.

[100] D. W. Boukhvalov and M. I. Katsnelson. Destruction of graphene by metal adatoms. *Appl. Phys. Lett.*, 95(2):023109, 2009.

[101] T. O. Wehling, M. I. Katsnelson, and A. I. Lichtenstein. Impurities on graphene: Midgap states and migration barriers. *Phys. Rev. B*, 80(8):085428, 2009.

[102] Olcay Uzengi Akturk and Mehmet Tomak. Bismuth doping of graphene. *Appl. Phys. Lett.*, 96(8):081914, 2010.

[103] Wei Zhang, Litao Sun, Zijian Xu, Arkady V. Krasheninnikov, Ping Huai, Zhiyuan Zhu, and F. Banhart. Migration of gold atoms in graphene ribbons: Role of the edges. *Phys. Rev. B*, 81(12):125425, Mar 2010.

[104] M. Klintenberg, S. Lebègue, M. I. Katsnelson, and O. Eriksson. Theoretical analysis of the chemical bonding and electronic structure of graphene interacting with group ia and group viia elements. *Phys. Rev. B*, 81(8):085433, Feb 2010.

[105] Simone Casolo, Ole Martin Lovvik, Rocco Martinazzo, and Gian Franco Tantardini. Understanding adsorption of hydrogen atoms on graphene. *J. Chem. Phys.*, 130(5):054704, 2009.

[106] Kun Xue and Zhiping Xu. Strain effects on basal-plane hydrogenation of graphene: A first-principles study. *Appl. Phys. Lett.*, 96(6):063103, 2010.

[107] Hayley McKay, David J. Wales, S. J. Jenkins, J. A. Verges, and P. L. de Andres. Hydrogen on graphene under stress: Molecular dissociation and gap opening. *Phys. Rev. B*, 81(7):075425, Feb 2010.

[108] L Pisani, B Montanari, and N M Harrison. A defective graphene phase predicted to be a room temperature ferromagnetic semiconductor. *New J. Phys.*, 10(3):033002 (9pp), 2008.

[109] Zheng Liu, Soon-Kil Joung, Toshiya Okazaki, Kazu Suenaga, Yoshiaki Hagiwara, Tetsu Ohsuna, Kazuyuki Kuroda, and Sumio Iijima. Self-assembled double ladder structure formed inside carbon nanotubes by encapsulation of h8si8o12. *ACS Nano*, 3(5):1160–1166, May 2009.

[110] J. A. Vergés and P. L. de Andres. Trapping of electrons near chemisorbed hydrogen on graphene. *Phys. Rev. B*, 81(7):075423, Feb 2010.

[111] A. J. Stone and D. J. Wales. Theoretical studies of icosahedral c_{60} and some related species. *Chem. Phys. Lett.*, 128:501–503, 1986.

[112] Y. Miyamoto, A. Rubio, S. Berber, M. Yoon, and David Tománek. Spectroscopic characterization of stone-wales defects in nanotubes. *Phys. Rev. B*, 69:121413(R), 2004.

[113] Elif Ertekin, D. C. Chrzan, and Murray S. Daw. Topological description of the stone-wales defect formation energy in carbon nanotubes and graphene. *Phys. Rev. B*, 79(15):155421, 2009.

[114] Takahiro Shimada, Daisuke Shirasaki, and Takayuki Kitamura. Stone-wales transformations triggered by intrinsic localized modes in carbon nanotubes. *Phys. Rev. B*, 81(3):035401, Jan 2010.

[115] Jie Ma, Dario Alfe, Angelos Michaelides, and Enge Wang. Stone-wales defects in graphene and other planar sp^2-bonded materials. *Phys. Rev. B*, 80(3):033407, 2009.

[116] O. Yazyev and S. Louie. Topological defects in graphene: dislocations and grain boundaries. *Phys. Rev. B*, 81(19):195420, 2010.

[117] Chuanhong Jin, Fang Lin, Kazu Suenaga, and Sumio Iijima. Fabrication of a freestanding boron nitride single layer and its defect assignments. *Phys. Rev. Lett.*, 102(19):195505, 2009.

[118] Jannik C. Meyer, Andrey Chuvilin, Gerardo Algara-Siller, Johannes Biskupek, and Ute Kaiser. Selective sputtering and atomic resolution imaging of atomically thin boron nitride membranes. *Nano Letters*, 9(7):2683–2689, July 2009.

[119] William A. McKinley and Herman Feshbach. The coulomb scattering of relativistic electrons by nuclei. *Phys. Rev.*, 74(12):1759–1763, Dec 1948.